**Technische Universität Berlin**

**Humboldt-Universität zu Berlin**

**Bernstein Center for Computational Neuroscience Berlin**




Master Thesis

# Noisy dynamics of a neuron with co-existing spiking and resting states

Tatiana Prudnikova

Matriculation Number: 367025

11.05.2018

Supervised by

Prof. Dr. Susanne Schreiber

HU Berlin

I declare in lieu of oath that I have written this thesis independently, without illicit assistance from third parties and using solely the aids mentioned.

Berlin, 11.05.2018

. . . . . .

*(Signature)*

**Abstract**

It is known that transition between resting and spiking states of a single neuron is in some cases associated with emergence of a limit cycle and simultaneous disappearance of resting state equilibria (e.g. a saddle-node on invariant circle bifurcation). We study a two-dimensional conductance based neuron model, which under certain parameter ranges has co-existing stable limit cycle and stable node, i.e. resting and spiking states exist at the same time. This can be reached through saddle homoclinic orbit bifurcation (also known as simply homoclinic bifurcation) by changing different parameters. In this work we use the time constant of potassium ion channel conductance. As we assume a noisy input to the neuron, the system can switch between resting and spiking states and thus execute different spiking patterns. We study transition between the patterns, show what different spiking timescales might be, and try to understand the shape of the interspike interval histogram.

**Zusammenfassung**

Es ist bekannt, dass der Übergang zwischen Ruhe- und spiking Zuständen eines Neurons manchmal mit der Enstehung von einem Grenzzyklus und gleichzietiger Verschwindung von Fixpunkten des Ruhezustands verbunden ist. Wir erforschen ein zweidimensionales auf Leitfaehigkeit basiertes Modell, das für einen bestimmten Parameterbereich co-existierend einen stabilen Knoten und einen stabilen Grenzzyklus hat, d.h. Ruhe- und spiking Zustaende existieren gleichzeitig. Das kann erreicht werden, indem verschiedene Parameter geändert werden. Wir nutzen dafür die Zeitkonstante der Leitfaehigkeit des Kaliumionenkanals. Wenn der Eingangström vom Neuron verrauscht ist, kann das System zwischen Ruhe- und spiking Zuständen wechseln und deshalb verschiedene spiking Musters ausführen. Wir untersuchen den Übergang zwischen den Musters, zeigen, wie unterschiedlich Interspikeintervalle sein können, und versuchen die Form vom Interspikeintervallhistogramm zu verstehen.

# Contents

# 1 Introduction

The saddle homoclinic orbit (homoclinic) bifurcation is the bifurcation that is characterized by the existence of a homoclinic orbit that starts at the saddle, follows its unstable manifold and goes back to the saddle through its stable manifold. When this bifurcation occurs at the same time with the saddle node bifurcation, the codimension-two saddle-node loop (SNL bifurcation, also known as saddle-node homoclinic orbit) bifurcation takes place (Figure 1). It was recently shown (Hesse et al. (2017)) that this bifurcation is common for a wide set of neuronal models and is usually caused by separation of dynamic variables time scales.

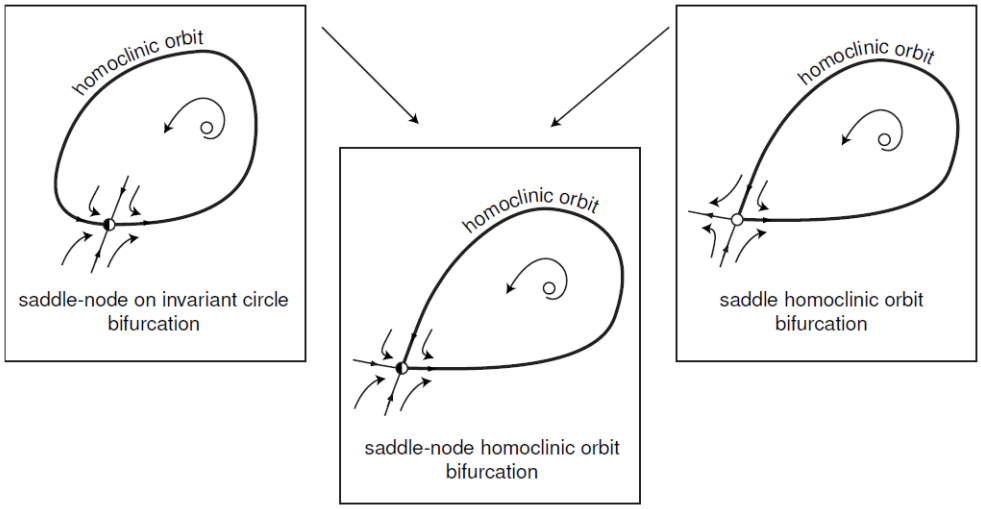


Figure 1: Saddle-node, saddle-node loop and saddle homoclinic orbit bifurcations. From Izhikevich (2007).

Saddle homoclinic orbit bifurcation can be of two types. Small homoclinic bifurcation is the one depicted on Figure 1, in this case the node of the

system lies outside the homoclinic trajectory. The second type is big homoclinic bifurcation, for which the homoclinic trajectory returns to the saddle from the other stable manifold and the node is inside the orbit. Among parameters causing SNL bifurcation occurrence are leak conductance (Kirst et al. (2015)), membrane capacitance (Hesse et al. (2017)) and time constant of potassium ion channel (Izhikevich (2007)).

While saddle node on invariant circle bifurcation switches the neuron from the resting behaviour to the tonic spiking, the saddle homoclinic orbit bifurcation leads to the phase plane with co-existing stable node and stable limit cycle, i.e. for the same parameters neurons can be either quiet or constantly firing. If there is a source of noise to the system, for a neuron with stable node and no limit cycle it would cause fluctuations around the node with occasional occurrence of single spikes. For bistable neuron, i.e. after passing the homoclinic bifurcation, arises the possibility for it to switch between the two stable regimes. Neuron can be quiet for a while, fluctuating around the node, or burst fluctuating around the limit cycle.

For neurons with stable node and no limit cycle the interspike interval (ISI) distribution corresponds to the escape rate from the node to the saddle and is thus described by an exponential distribution (Chow and White (1996)). After the neuron passes the saddle node on invariant circle bifurcation and starts firing constantly, the distribution of ISIs can be described by the inverse gaussian (Schwalger et al. (2010)).

For neurons that alternate between bursting and quiescence, the ISI distribution is often bimodal. It can be observed for example in the recordings from dopamine neurons (Robinson et al. (2004)), neurons of V1 and LGN

(Christen et al. (2004)), cholinergic interneurons (Bennet and Wilson (1999)) etc. In this case the first mode of the ISI distribution usually corresponds to ISIs within bursts (further referred to as burst ISIs) and the second mode to ISIs between bursts (further referred to as quiet ISIs). It is important to mention though, that bimodal ISI distribution doesn't always mean that the neuron has a bursting behaviour, and bursting neurons don't always have bimodal ISI distributions (Shi (2005)).

The purpose of this work was to study the behaviour of particular neuronal model, for which SNL (i.e. also saddle homoclinic orbit) bifurcation occurs, in the area of bistability, examine its bursting characteristics, and ISI distribution.

# 2 Model and Methods

We study two-dimensional persistent sodium plus potassium ($I_{Na,p} + I_K$) neuron model:

$$CV' = I - I_L - I_{Na,p} - I_K + \mu_{I_{noise}} \quad (1)$$

$$I_L = g_L(V - E_L) \quad (2)$$

$$I_{Na,p} = g_{Na} m_\infty(V)(V - E_{Na}) \quad (3)$$

$$I_K = g_K n(V - E_K) \quad (4)$$

$$n' = (n_\infty - n)/\tau_n \quad (5)$$

$$n_\infty = \frac{1}{1 + e^{(-25-V)/5}} \quad (6)$$

$$m_\infty = \frac{1}{1 + e^{(-20-V)/15}} \quad (7)$$

$$C = 1\mu F/cm^2$$
$$g_L = 8mS/cm^2$$
$$g_{Na} = 20mS/cm^2$$
$$g_K = 10mS/cm^2$$
$$E_L = -80mV$$
$$E_{Na} = 60mV$$
$$E_K = -90mV$$

This model takes into account that opening and closing of $Na$ ion channels is much faster than $K$ ion channels dynamics, so we can assume that $m$ reaches $m_\infty$ immediately.

We know that the speed of ion channel dynamics is not constant but depends for example on such physiological parameter as temperature (Lee (1990)). If we treat the time constant of gating variable $\tau_n$ and applied external current $I$ as bifurcation parameters, we get the bifurcation diagram on Figure 2.

The vertical line $I = 4.51$ on Figure 2 corresponds to saddle-node bifurcation. For $\tau_n$ greater than 0.17 when the system crosses saddle-node bifurcation line (Figure 3) a stable limit cycle emerges and the system switches

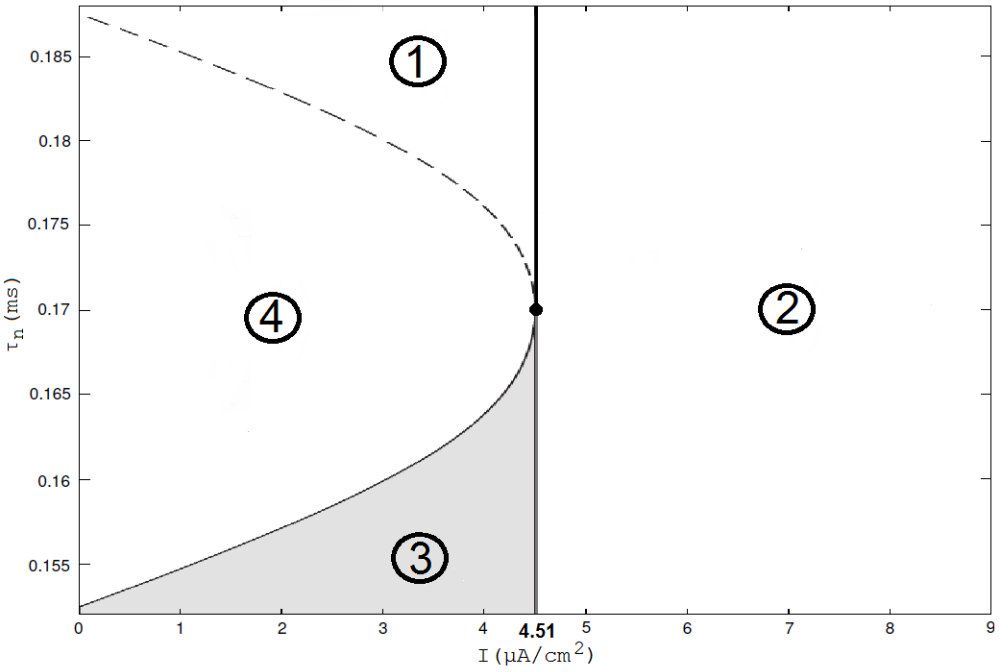


Figure 2: Bifurcation diagram of $I_{Na,p} + I_K$ neuron.

from being quiet on the left side of the line (area 1 on Figure 2) to executing tonic spiking on the right side (area 2 on Figure 2).

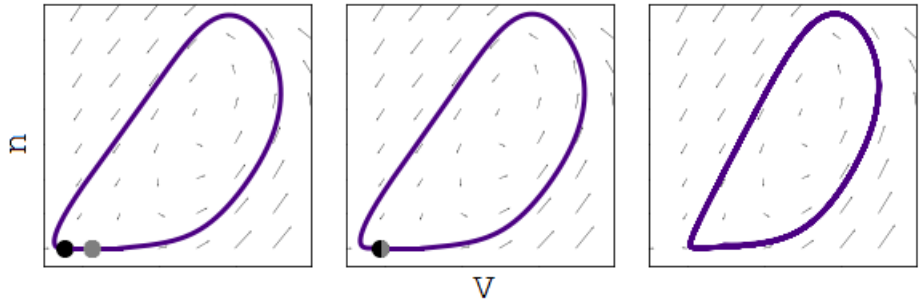


Figure 3: From area 1 to area 2. Saddle-node on invariant circle bifurcation.

Above the dashed line (area 1 on Figure 2) the trajectory, that leaves

the saddle in the direction of the right unstable manifold terminates at the node, reaching the node from its left strongly stable manifold. At the dashed line (Figure 4) this trajectory goes into the node through it's weakly stable manifold. And below the dashed line (area 4 on Figure 2) it approaches the node from the right strongly stable manifold.

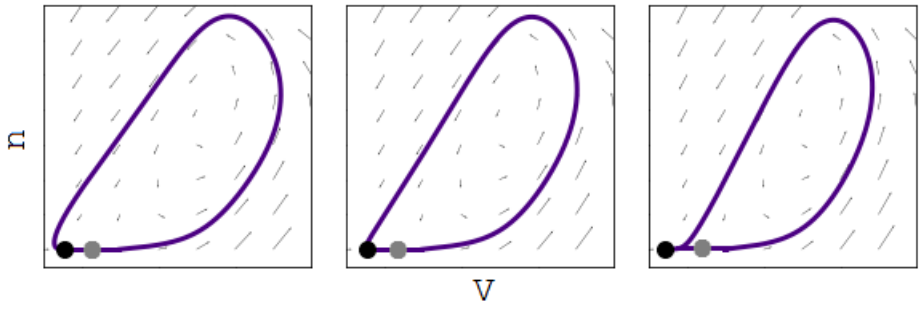


Figure 4: From area 1 to area 4. Heteroclinic orbit approaches the node from a different manifold.

The last line on Figure 2 corresponds to pairs of parameters $\tau_n$ and $I$ for which the trajectory leaving the saddle along its unstable manifold terminates also at the saddle, reaching it along the stable manifold (Figure 5). To the right from this line (area 3 on Figure 2) a stable limit cycle emerges, and the trajectory, that goes from the saddle along its unstable manifold, gets attracted by this limit cycle.

For $\tau_n$ smaller than 0.17 when $I$ reaches the value of 4.51 the saddle and the node collide and then disappear (Figure 6). The limit cycle is the only attractor on the phase plane and the system is constantly spiking (area 2 on Figure 2).

The region, that we are interested in, is the region of bistability, grey

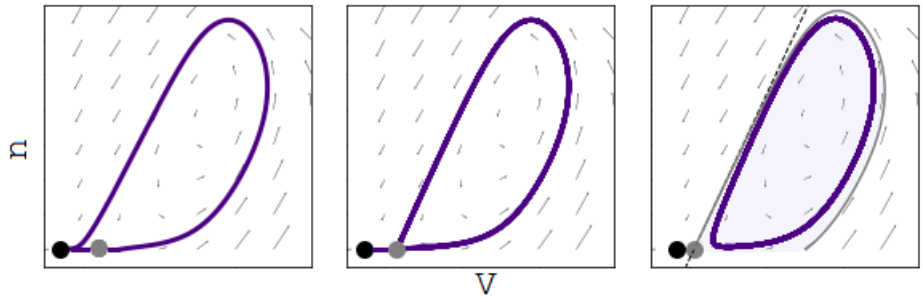


Figure 5: From area 4 to area 3. Saddle homoclinic orbit bifurcation.

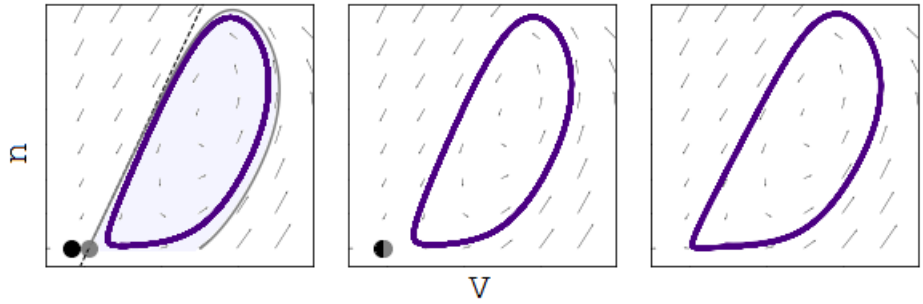


Figure 6: From area 3 to area 2. Saddle-node off limit cycle bifurcation.

shaded area 3 on Figure 2. As we mentioned, in this region stable node (lower state) co-exists with stable limit cycle (upper state). In the lower state the neuron is quiet, in the upper state the neuron is spiking. There are two other unstable fixed points on the phase plane. One is the unstable focus inside the limit cycle, the other is the saddle. The stable manifold of the saddle acts as a separatrix, dividing the phase plane into regions of attraction (see the leftmost plot on Figure 6). Every trajectory, starting exactly on the separatrix, terminates at the saddle. Every trajectory, with starting point in the purple shaded area on the leftmost plot on Figure 6,

ends up at the limit cycle. All other trajectories terminate at the node.

There are many sources of noise in biological neurons, for example ion channels are noisy (Hille 1992). If we introduce noise to our system we might observe jumping over the separatrix, i.e. switching to the other region of attraction. Therefore we can observe the system alternating between spiking and quiet regimes. We want to simulate the model for various parameters, which guarantee the existence of bistability, look at the trajectories, and understand how executing two different behaviour patterns is reflected in the overall ISI distribution. We would expect the ISI distribution to look bimodal, since it is often the case for bursting neurons.

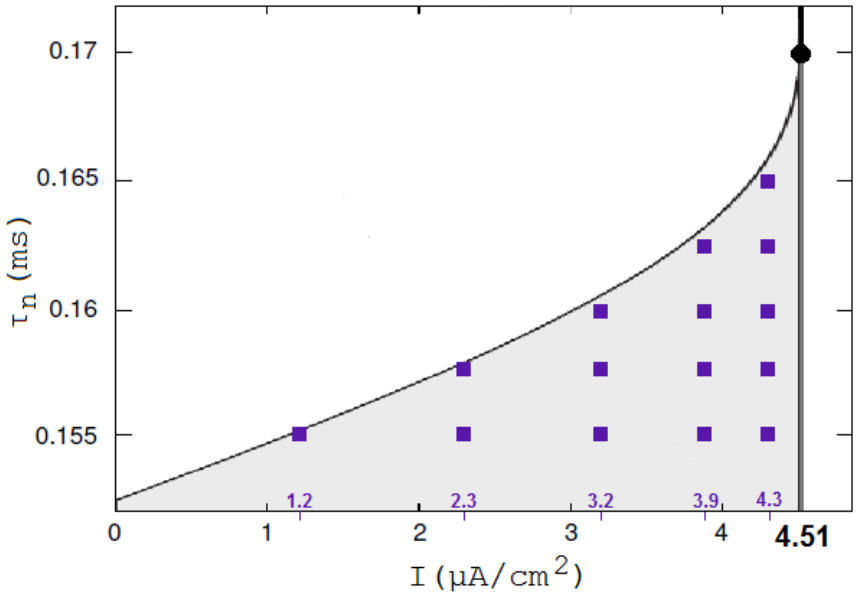


Figure 7: Pairs of the parameters selected for simulations and analysis.

First of all we should study how changing the parameters affects the phase portrait. We know the area on the parameters plane where the neuron

is bistable: it is limited by the straight line on the right, and by the branch of the parabola on the left. We cover this area with a non-uniform grid as follows: we increase $\tau_n$ uniformly, choosing the following values: 0.155ms, 0.1575ms, 0.160ms, 0.1625ms, 0.165ms and we take $I$ values close to the corresponding homoclinic bifurcation points. We end up with the grid represented at Figure 7. We also take three different noise levels, for which alternating between the two regimes takes place: $2\mu$A, $2.5\mu$A, $3\mu$A to study how noise strength affects the dynamics.

When calculating statistics and plotting the results we approximated the separatrix with a straight line going through the saddle in the direction of the the eigenvector corresponding to its stable manifold (dotted line on the leftmost plot on Figure 6). As can be seen on Figure 6 in the proximity of the saddle the separatrix is indeed close to being linear.

When simulating the noiseless system we encountered the problem that normally used time step was too big to get valid results for parameters close to the homoclinic bifurcation. We think that the reason is that the homoclinic bifurcation is not typical existence/non-existence, stability/unstability of an attractor bifurcation. The limit cycle and the separatrix are very close to each other and at each step of the simulation making a slightly bigger jump might bring the system to the wrong side of the separatrix. That's why for plotting phase planes in the vicinity of homoclinic bifurcation line we took the time step of $5 \times 10^{-5}$ms. For noisy simulations we didn't see any difference when working with smaller time step, so we took the time step of $1 \times 10^{-3}$ms.

We ran the simulations using the Brian2 simulator.

# 3 Results

First of all we studied how bifurcation parameters $\tau_n$ and $I$ affect the phase plane. We identified the node, the saddle and the limit cycle, as well as the linear approximation of the separatrix, for different pairs of the parameters from the grid depicted on Figure 7.

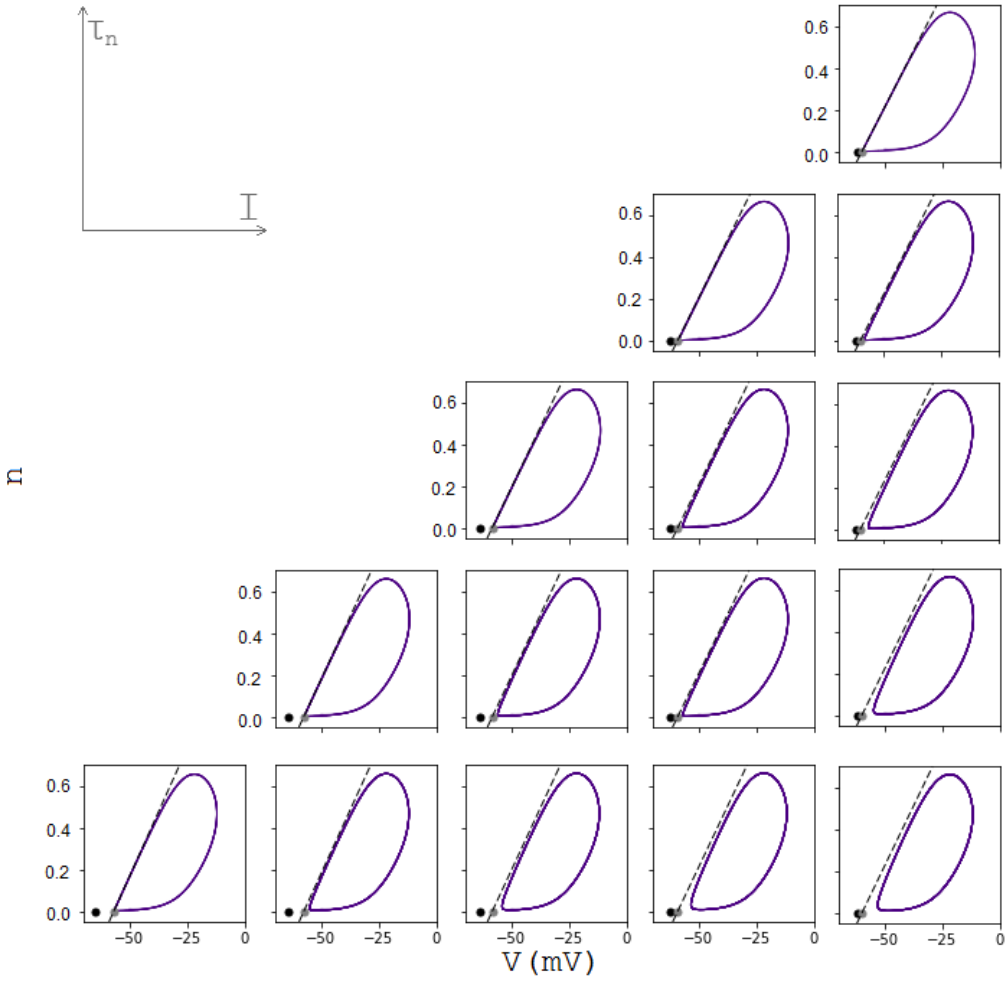


Figure 8: Phase planes for the selected parameters' pairs.

On Figure 8 one can see that as expected for a fixed $\tau_n$ increasing the applied current $I$ brings the saddle and the node closer together with both of them moving towards each other, until they collide at the saddle-node bifurcation line. At the same time the limit cycle and the saddle (also the separatrix), are close to each other next to the homoclinic bifurcation line and move further apart with the increase of $I$. So when the noise is applied to the system we would expect that it gets harder to switch from the spiking regime to the quiet regime and easier to switch from the quiet regime to the spiking regime when $I$ is increased.

When fixing $I$ and increasing $\tau_n$-value, the saddle and the node don't move, since $\tau_n$ is only the scaling factor in the differential equation (5), which describes the $n$ variable dynamics, so it doesn't affect the location of the fixed points of the system. At the same time it affects the limit cycle, bringing it closer to the saddle with the increase of $\tau_n$.

It is important to notice that the separatrix approximation for the small values of $n$ is quiet precise. As we know the true separatrix goes around the limit cycle, i.e. at some point bends to the right from its linear approximation. At the same time it doesn't cross the limit cycle, which means that it is locked between the limit cycle and the linear approximation. For the parameters close to the homoclinic bifurcation one can visually see no gap between them for $n$-values in the range from 0 to roughly 0.5. Further from the homoclinic bifurcation line this gap increases, but for $n$-values around 0.5 they are still close, so for $n$-values below 0.5 the true separatrix can't be drastically different from its linear approximation.

Now that we have the idea of how the noiseless system works, we run

several simulations to see how noise can affect its behaviour. We start by examining the traces.

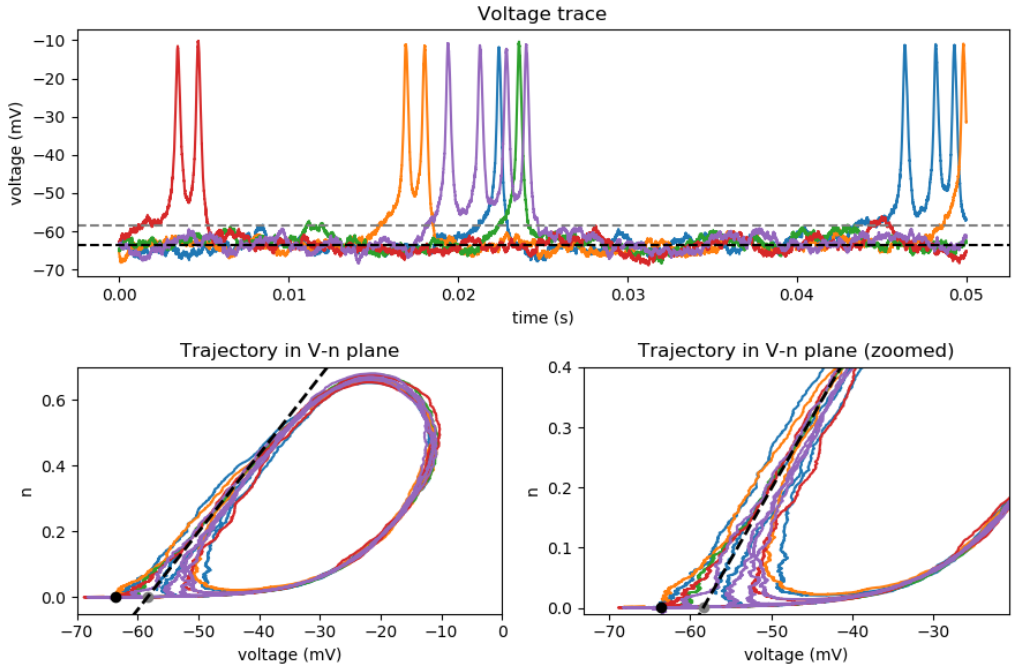


Figure 9: Examples of voltage and $V$-$n$ traces. On the upper plot grey dotted line represents the saddle and black dotted line represents the node.

On Figure 9 we plot $V$ and $V$-$n$ traces for five neurons with the same parameters values simulated for 50ms. We can see that they all perform bursting, but the number of spikes in the burst and the duration of interburst intervals varies. The $V$-$n$ trajectories also show diversity, with the area around the separatrix being densely covered with different trajectories.

On Figure 10 we can see the result of two simulations of the system with parameters $\tau_n = 0.1575$ms, $I = 2.3\mu\text{A}/cm^2$, $\mu_{I_{noise}} = 2.5\mu\text{A}/cm^2$ and initial point $V_0 = -50$mV, $n_0 = 0.01$ for 2.5ms. Though the trajectories

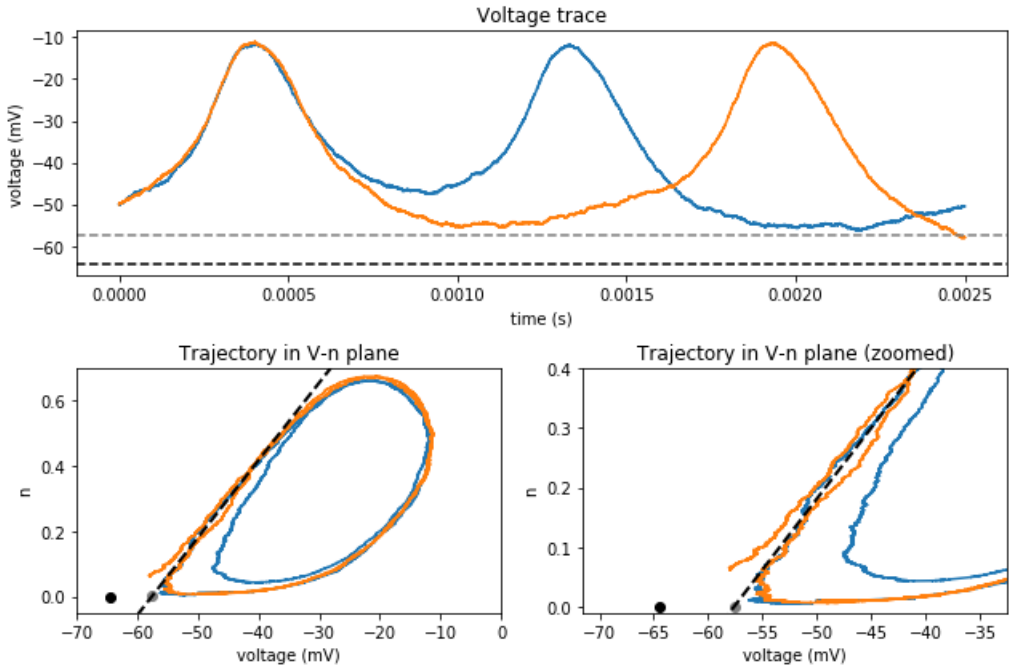


Figure 10: Examples of trajectories that lead to repetitive spiking.

after the first spike look different, both of them eventually lead to spiking again without going to the node. The blue trajectory is located inside the limit cycle leading to smaller ISI, while the orange one follows the separatrix, approaches the saddle and only then goes back up, making the ISI longer.

On Figure 11 we can see another two simulations for the same parameters, the same initial point and the same duration. This time both of them at some point get to the node and then have to escape its attraction to fire again. We can notice that the orange trajectory follows the separatrix for some time, gets close to the saddle and only then goes to the node, while the blue one crosses the separatrix quite early and then goes in the direction of the node, never approaching the separatrix again. In the observed time interval both

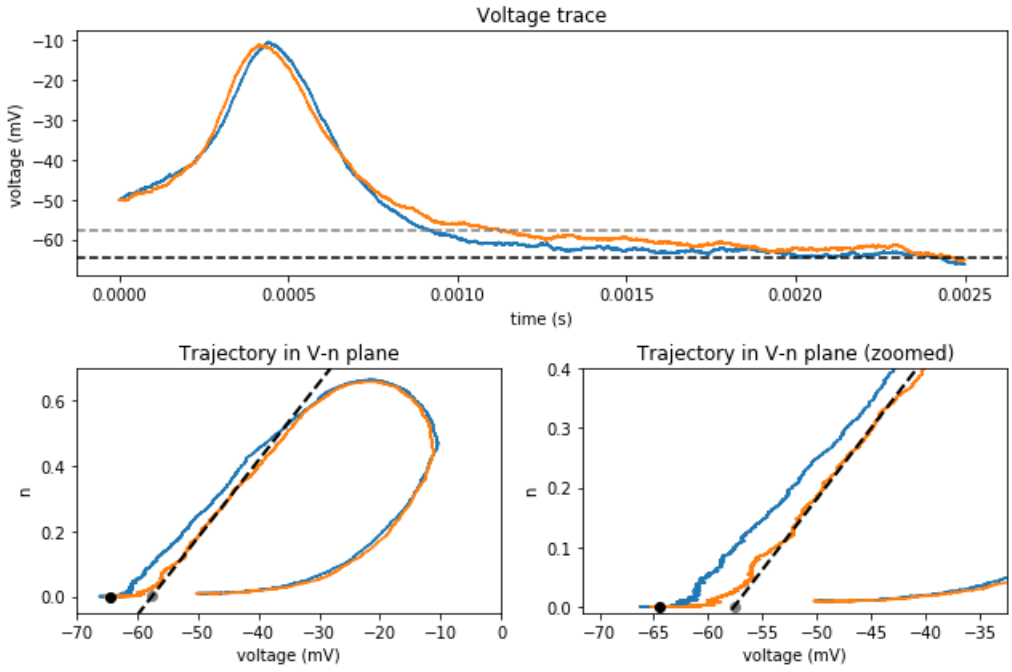


Figure 11: Examples of trajectories that lead to the resting state.

neurons fired only once and they both need time to overcome the potential barrier between the node and the saddle to fire again. This leads to longer quiet ISIs.

Now we take the selected parameters pairs and levels of noise and run simulations for ten neurons and the duration of 50 seconds, in order to collect data for statistical analysis. The initial values of V and n were distributed randomly around the saddle. We present plots for the noise strength $3\mu$A. Plots for the other noise levels can be found in the appendix.

In our further calculations we have to classify ISIs into burst and quiet (i.e. the ones that spend some time around the resting state) ISIs. This classification is somewhat arbitrary, since it's not clear what exactly being

around the resting state means. We took minimal values of the voltage within the ISIs as a decisive parameter, calling an ISI quiet if the minimal voltage is smaller than $V_{node} + 0.1 \times (V_{saddle} - V_{node})$, and calling it burst ISI otherwise. When the voltage reaches this value from above, we say that the trajectory reaches proximity of the node. With this classification all ISIs classified as quiet include most of the distance between the node and the saddle.

We also introduce two additional notions:

1. "crossing down" - the moment within a quiet ISI when the trajectory crosses the separatrix (approximation) for the last time before reaching the proximity of the node for the first time, i.e. the moment when the neuron leaves the limit cycle's region of attraction for the last time.

2. "crossing up" - the moment within a quiet ISI when the trajectory crosses the separatrix (approximation) for the last time before spiking, i.e. the moment when the neuron leaves the node's region of attraction for the last time.

Since we already know that trajectories reaching proximity of the node can be quite different, we plotted histograms of $n$-values at moments of "crossing up" and "crossing down" for different parameters' pairs. Since we use linear approximation of the separatrix, voltage histograms would look the same, but shifted and scaled. For noise level $\mu_{I_{noise}} = 2\mu\text{A}/cm^2$ and parameters $\tau_n = 0.155\text{ms}$ and $I = 1.2\mu\text{A}/cm^2$ number of quiet ISIs is small, so the histograms are not informative and hence not included in plots and analysis.

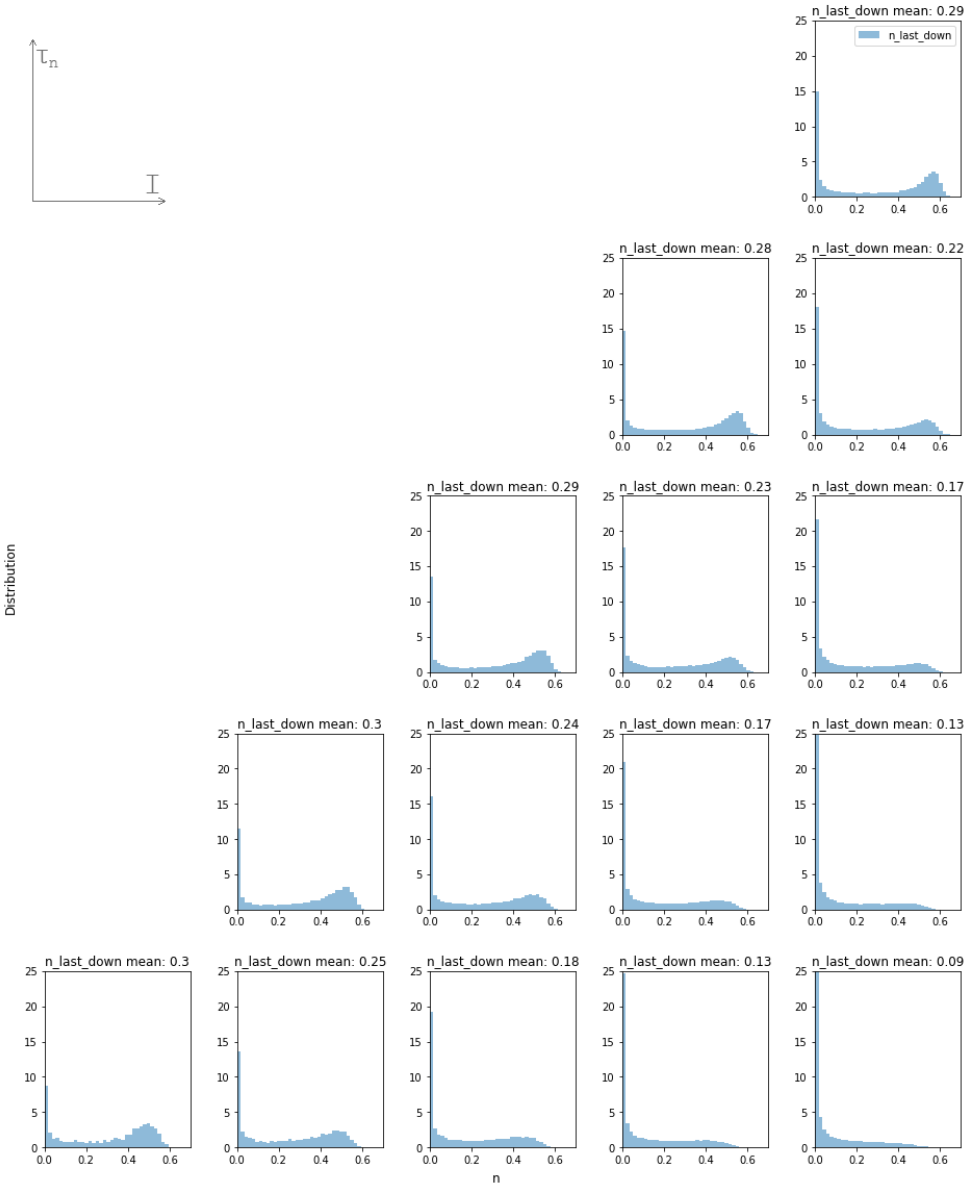


Figure 12: Distributions of $n$-values at "crossing down" points for the selected parameters' pairs and $\mu_{I_{noise}} = 3\mu\text{A}/cm^2$.

For the "crossing down" values on Figure 12 we can see that further from the homoclinic bifurcation line the distribution has a strong single mode close to zero, i.e. close to the saddle. A lot of trajectories leading to the node first get attracted by the saddle and only afterwards go to the node. At the same time the lowest mean crossing point is at 0.09, so there are still many trajectories that turn to the saddle earlier, but the "crossing down" points are spread along the separatrix.

As we get closer to the homoclinic bifurcation line, the second peak of the distribution emerges. This means that there are two distinct types of trajectories: the ones that get attracted by the saddle first, and the ones that cross the separatrix quite early and go to the node directly from there. As we can see the second mode is around $n = 0.5$, and it gets more and more pronounced the closer we get to the homoclinic bifurcation line. The mean values of $n$ also grow and reach roughly 0.3 for parameters values close to the homoclinic bifurcation.

We always have to remember though that what we call "the separatrix" is only its linear approximation. However, we know from the phase plane plots on Figure 8 it is good at least for $n$-values below 0.5. Additionally, any trajectory crosses the true separatrix first. So if it crosses approximation line far from the saddle (i.e. when $n$ is far from zero), it also crosses the true separatrix far from the saddle, since$n$-values in proximity of the saddle can't increase.

For the "crossing up" (Figure 13) there is much less variability in $n$-values. For any set of parameters distribution has small mean and small variance, which grow slightly for points further from the saddle-node bifurcation. This

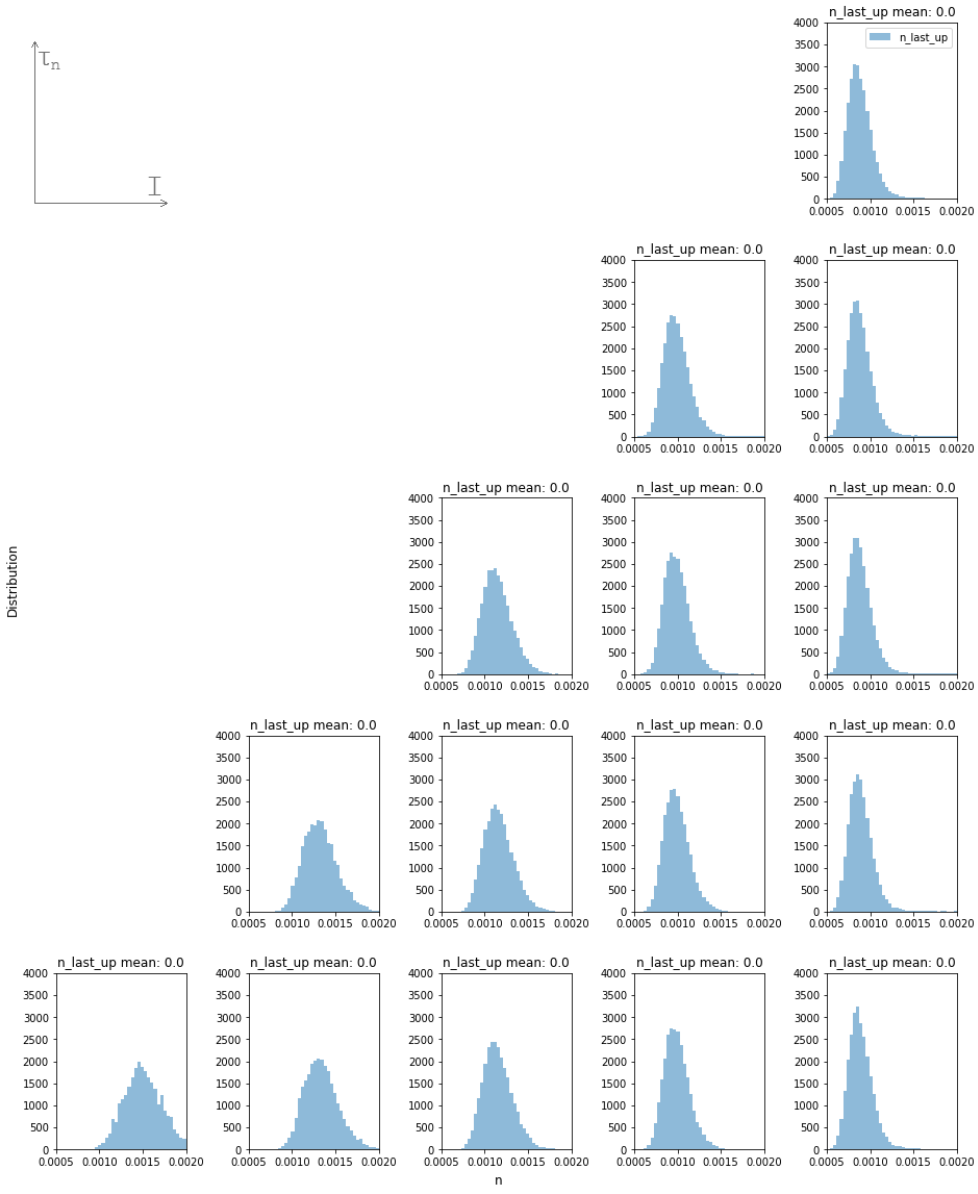


Figure 13: Distributions of $n$-values at "crossing up" points for the selected parameters' pairs and $\mu_{I_{noise}} = 3\mu\text{A}/cm^2$.

means that when escaping from the node all trajectories go roughly horizontally and cross the separatrix close to the saddle. The distribution is unimodal and approximately Gaussian.

Now let's look at the ISI distributions. As said before, we expected to observe bimodal ISI distribution, since the system has two firing patters: bursting and firing after spending time around the resting state. We cut off the histograms at 20ms since it was hard to see anything for larger values. Using the same range of values also makes it easier to compare ISI distributions to each other.

On Figure 14 we don't observe bimodal ISI distribution for any set of parameters. There's always a peak in the low range, around 1-2ms, and then the density decreases rapidly. At some point this decrease becomes much slower and stays slow for the long range of ISIs. Since density of the samples in these long "shoulders" of distributions is so small compared to the initial peak, we will later plot the same histograms with logarithmic scale on the y-axis to make visual investigation possible.

Although even with this visualization we can make several observations. We can see that the overall number of spikes increases with the increase of applied current $I$ and decreases with the increase of $\tau_n$ value. Larger noise leads to the larger average firing rate. The peak is very pronounced for low $\tau_n$ values and gets smaller for larger $\tau_n$. At the same time the effect of applied current on the shape of the peak is much smaller.

Mean ISI values vary a lot, with the smallest being only 2ms and the largest being 126ms for the noise of $3\mu$A and even larger for smaller noise intensities. Also we should notice that for most of the histograms the mean

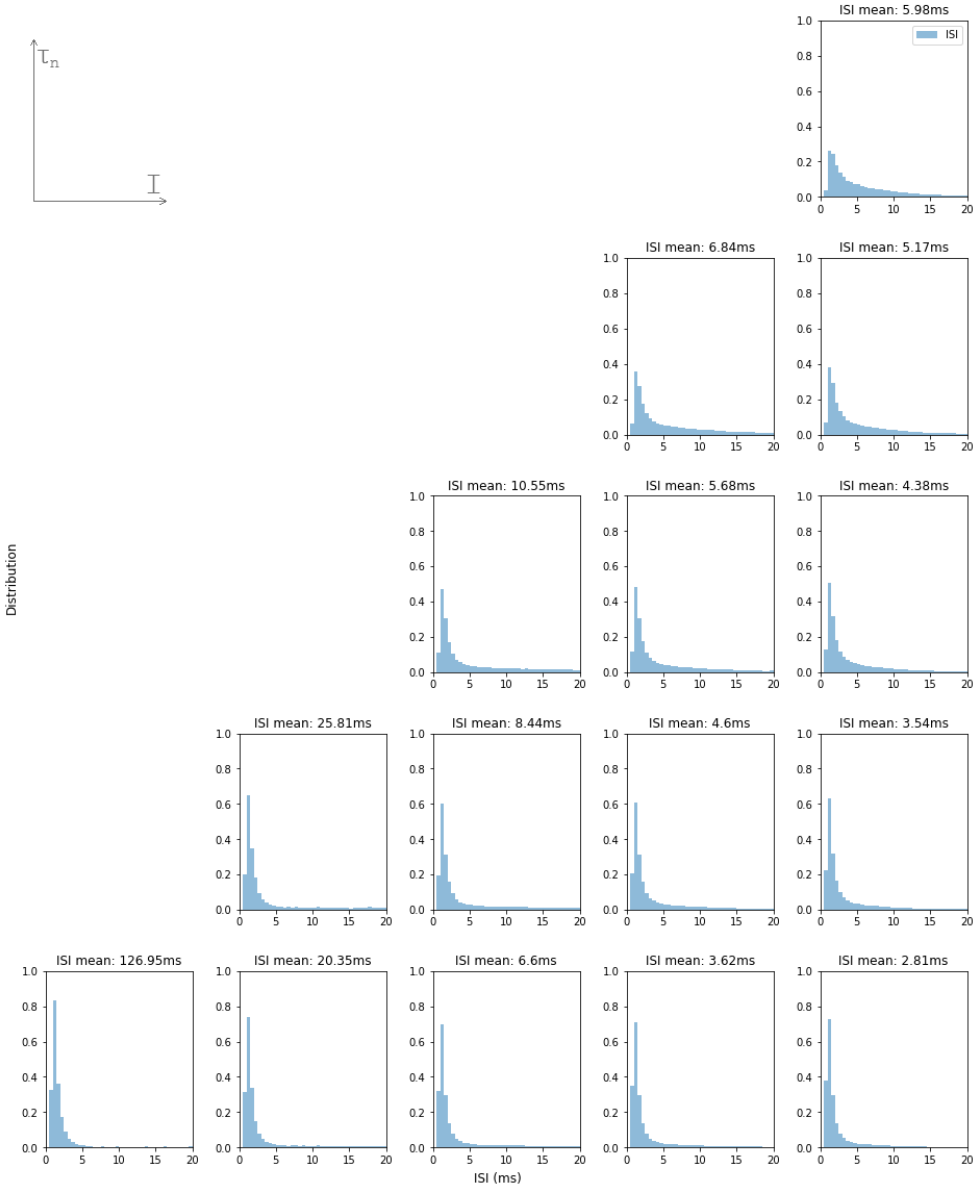


Figure 14: Overall distributions of ISIs for the selected parameters' pairs and $\mu_{I_{noise}} = 3\mu\text{A}/cm^2$.

value is far from the peak value, which is another indicator that a significant number of samples are located in the long "shoulders". To investigate them we plot logarithmic histograms.

On the logarithmic histograms on Figure 15 we can see that each distribution consists of two parts. The first part is the initial peak of the distribution followed by short fast decay. The second part corresponds to the "shoulder" of the distribution. For small $I$ values there is not enough samples in the shoulder so the histogram is noisy and it's hard to infer anything about its shape. But for larger $I$ values the "shoulder" looks linear. A smooth transition between these two parts occurs always around 5ms ISIs.

For larger $\tau_n$ values initial peak is smaller, and the "shoulder" is higher. That means that with the increase of $\tau_n$ fraction of samples belonging to the "shoulder" grows. At the same time with the increase of applied current $I$ the "shoulder" decays faster, i.e. the samples in the shoulder are less spread.

To investigate why the ISI distributions look the way they do we plotted quiet and burst ISI histograms together on Figure 16.

We know that for bursting neurons with bimodal ISI distribution the first mode of the distribution corresponds to the mode of the burst ISI histogram and the second mode corresponds to the mode of the quiet ISI histogram. On Figure 16 we can see that the single mode of the ISI distributions we observed corresponds as expected to the mode of the burst ISIs. At the same time the mode of the quiet ISIs is not represented in the overall ISI distributions.

The quiet ISI distributions vary a lot over the parameters' space. The peak is most pronounced for parameters close to the saddle-node bifurcation line. With decay of the applied current the distribution becomes more and

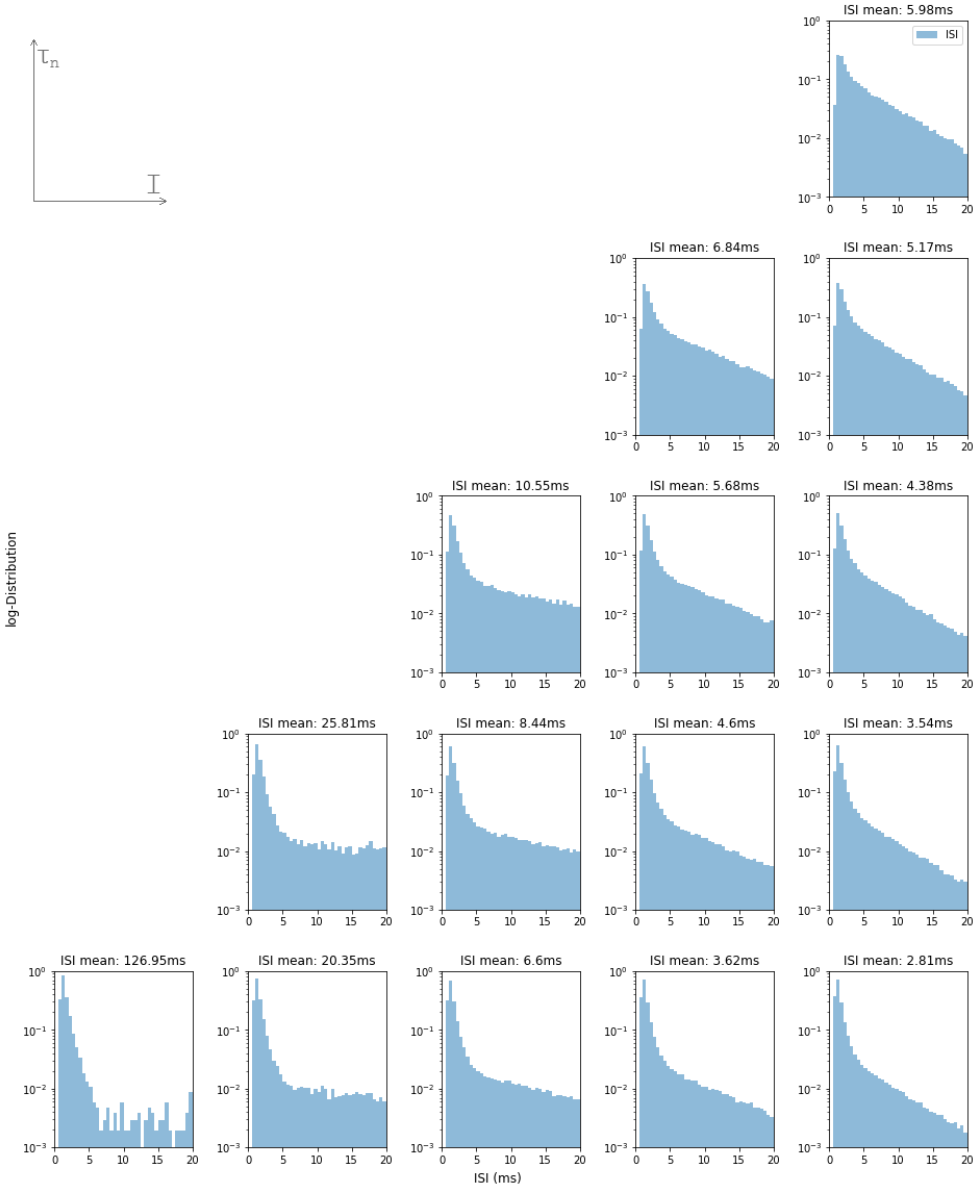


Figure 15: Overall log-distributions of ISIs for the selected parameters' pairs and $\mu_{I_{noise}} = 3\mu\text{A}/cm^2$.

more flat. $\tau_n$ doesn't affect the mean or the shape of the quiet ISI distribution that much, but decrease in the applied current leads to rapid growth of the mean with the smallest being around 9ms and the largest being 256ms. For smaller noise levels this difference is even larger. At the same time the position of the peak almost doesn't change. It is located at around 5ms for all histograms going slightly up with the decrease in the applied current.

The burst ISI distribution is less diverse with the mean around 1.5-2.5ms for all histograms and the peak close to zero. We will look at these distributions later in more detail.

We have two separate distributions with separate peaks, why don't we see the second mode in the overall ISI distribution?

The first factor is that the mode of the quiet ISI distribution is always small, which leads to the significant overlap in the distributions for big values of $\tau_n$ and the applied current $I$ (i.e. the upper right corner on Figure 16). The second factor is that when $\tau_n$ is small and $I$ value is large (i.e. lower right corner on Figure 16) the number of burst ISIs is much larger than the number of quiet ISI. So even though the overlap between the histograms is not so big, the number of burst ISIs in this area is still enough to "mask" the peak of the quiet ISI distribution. The last factor is that the peak of the quiet ISI distribution is not pronounced for small values of $\tau_n$ and $I$ (i.e. in the lower left corner on Figure 16).

Now let's briefly look at the distributions of burst ISIs.The applied current $I$ value doesn't affect the histograms a lot, the peak gets slightly larger and narrower for larger $I$ and interestingly the mean gets smaller with the growth of $I$ everywhere except in the lower left corner of Figure 16. Same applies

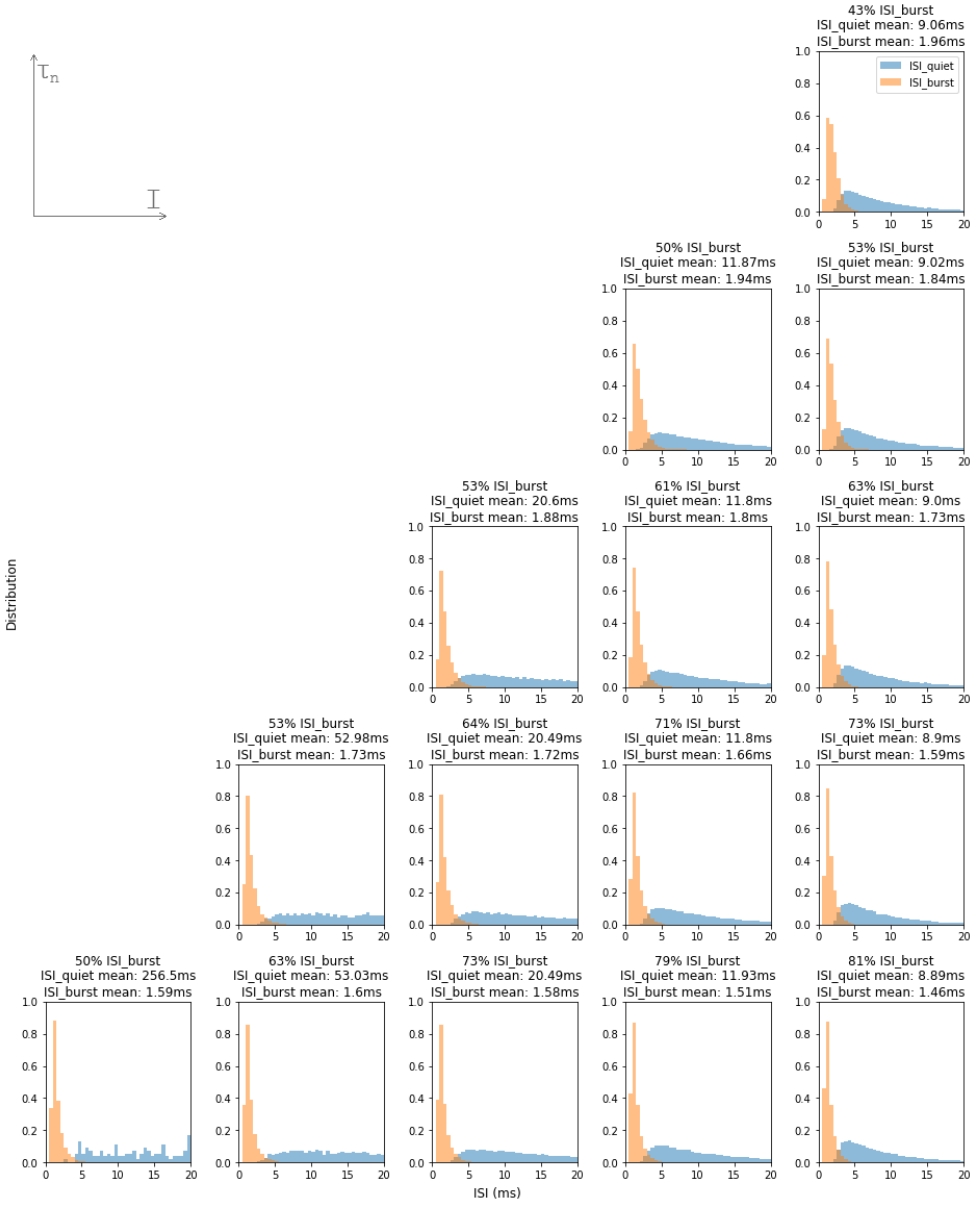


Figure 16: Distributions of quiet and burst ISIs for the selected parameters' pairs and $\mu_{I_{noise}} = 3\mu\text{A}/cm^2$.

to the other two noise levels. The effect of $\tau_n$ is more prominent. For large $\tau_n$-values the peak gets lower and wider, and the mean of the distribution grows.

As we saw quiet ISIs are on average much longer than burst ISIs. The initial explanation would be that this difference is mostly determined by the time it takes the neuron to escape the proximity of the node and reach the separatrix again. To investigate what really determines the length of a quiet ISI we divided each quiet ISI into following segments:

1. Time above - the time from spiking until crossing the separatrix for the last time on the way down ("crossing down") + the time it takes after crossing the separatrix for the last time on the way up ("crossing up") until the next spike, where we denote "way down" about the neuron going to the proximity of the node after spiking and "way up" about the remaining part of a quiet ISI.

2. Time down - the time it takes neuron to reach the node's proximity after "crossing down".

3. Time up - the time from reaching the proximity of the node until "crossing up".

We expected to observe that quiet ISI is roughly the sum of the "time up" and "time above", since during "time down" the neuron follows the vector field direction and thus it should be very small, i.e. neglectable in comparison to the other two segments.

We plotted the histograms of the three segments on Figure 17. As one can see the "time up" indeed dominates for all sets of parameters. At the

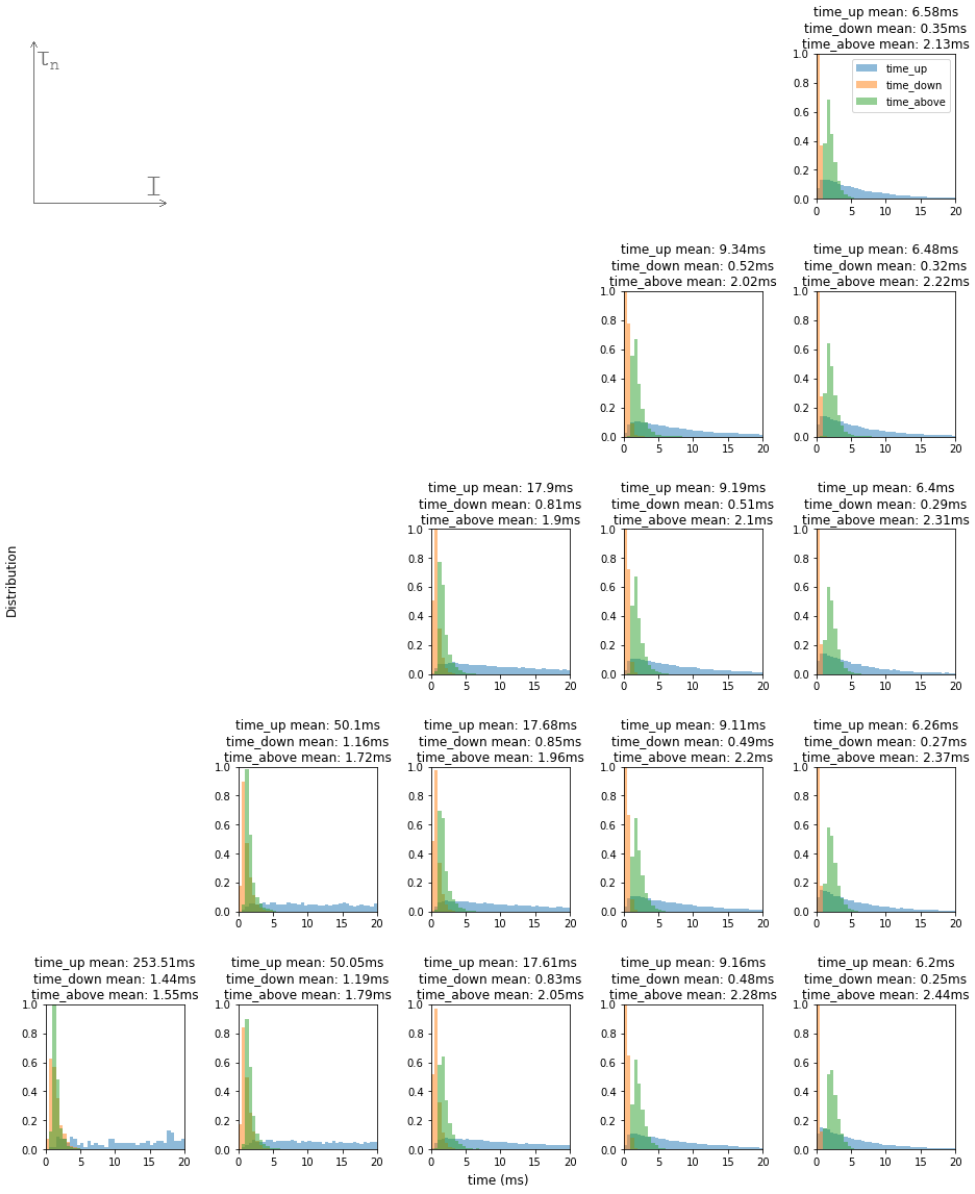


Figure 17: Distributions of quiet ISIs' segments for the selected parameters' pairs and $\mu_{I_{noise}} = 3\mu\text{A}/cm^2$.

same time whilst for small values of applied current $I$ (lower left corner on Figure 17) "time up" can be orders of magnitude larger than both other segments (especially for smaller noise values, see plots in the appendix), larger applied current $I$ leads to "time above" being comparable to "time up", though still smaller. For small applied current $I$ not only the "time up" becomes dominant, but also the "time down" grows and reaches almost the same values as "time above". So further from the saddle-node bifurcation "time up" is large and the other two segments are magnitudes smaller but comparable to each other. Closer to saddle-node bifurcation we have "time up" and "time above" of the same magnitude with the first being larger, and "time down" of lower magnitude. The effect of $\tau_n$ seems to be much smaller and doesn't influence the histograms a lot.

# 4 Discussion

1. When we just started studying ISI distributions for neurons with co-existing stable node and stable limit cycle, we used a more complicated Wang-Buzsaki model with three dynamic variables. We switched to the simpler two-dimensional $I_{Na,p} + I_K$ persistent sodium plus potassium model to make a detailed study of the system's behaviour easier. But before doing that we already produced ISI histograms and the results were similar to what we later observed for the two-dimensional model.

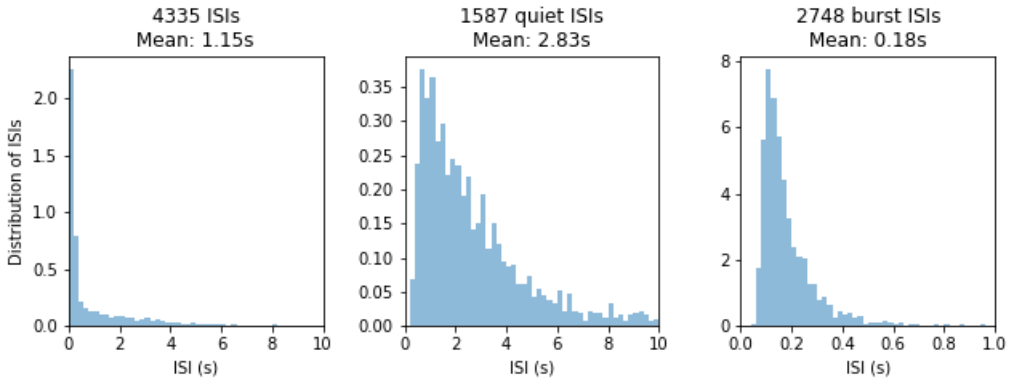


Figure 18: Examples of overall distribution of ISIs, distribution of quiet ISIs and distribution of burst ISIs for Wang-Buzsaki model.

On Figure 18 one of the produced histograms is presented. We can see that for the overall ISI distribution only a single initial peak exists and the distribution has a similar "shoulder". Quiet ISIs have a wide spread in duration and are on average much longer than burst ISIs. Burst ISIs are densely distributed around their mean and significantly exceed quiet ISIs in numbers. We thus hope that the results may generalize to higher dimensional neuron

models.

That brings us back to the note we made in the introduction about the connection between bursting behaviour of a neuron and bimodality of its ISI distribution. In this work we showed two models for which bursting behaviour doesn't imply a two-peaked ISI distribution. The peak corresponding to the mode of the bursting regime is there, but the mode of the quiet regime is not represented. As we also mentioned, bimodal distribution of ISIs doesn't necessarily imply underlying bursting. One has to be careful when trying to connect the two.

2. Another goal we had in the beginning was to find an analytical approximation of the overall ISI distribution. The idea was to approximate the burst ISI distribution with the distribution of periods of the system that oscillates following the limit cycle with fluctuations caused by noise. This distribution is known to be inverse gaussian (Schwalger et al. (2010)). As for quiet ISIs, we wanted to neglect the "time down" part and approximate it as a sum of the bursting part and escaping the node part, which is known to have exponential distribution (Chow and White (1996)).

First of all, as we showed in the results, the "time down" part is not always much smaller than the "time above" part, even though it is always small compared to the total ISI length being at most around 1/20 of the "time up". We don't go too close to the saddle-node bifurcation line where this difference might be smaller.

Next, we tried to fit exponential distribution to the "time up" part. It worked nicely and only had a small gap between the distribution in the low range (see Figure 33 in the appendix). The burst ISIs and the "time

above" distributions are more similar to each other close to the homoclinic bifurcation line (see Figure 36 in the appendix), but they are still quite different. The burst ISI distribution can be approximated by the inverse gaussian close to the SNL bifurcation point (Figure 39). While for "time above" distribution the good fit can be achieved next to the saddle-node bifurcation line, but it is the best further from the SNL bifurcation point (Figure 42).

To sum up, it seems that the analytical approximation could be found for the parameters close to the SNL point if we neglect the "time down" part and make two different inverse gaussian approximations for burst ISI and "time above" distributions.

# 5 Bibliography


1. Hesse, J., Schleimer, J.-H., Schreiber, S., 2017. Qualitative changes in phase-response curve and synchronization at the saddle-node-loop bifurcation. PHYSICAL REVIEW E 95

2. Izhikevich, E.M., 2007. Dynamical Systems in Neuroscience:The Geometry of Excitability and Bursting. The MIT Press

3. Kirst, C., Ammer, J., Felmy, F., Herz, A., Stemmler, M., 2015. Fundamental Structure and Modulation of Neuronal Excitability: Synaptic Control of Coding, Resonance, and Network Synchronization. bioRxiv preprint, 2015

4. Chow, C.C., White, J.A., 1996. Spontaneous Action Potentials due to Channel Fluctuations. Biophysical Journal Volume 71, 1996 3013-3021

5. Schwalger, T., Fisch, K., Benda, J., Lindner. B, 2010. How Noisy Adaptation of Neurons Shapes Interspike Interval Histograms and Correlations. PLoS Computational Biology, Volume 6, Issue 12

6. Robinson, S., Smith, D.M., Mizumori, S.J.Y., Palmiter, R.D., 2004. Firing properties of dopamine neurons in freely moving dopamine-deficient mice: Effects of dopamine receptor activation and anesthesia. PNAS, vol. 101, no. 36, 13329 –13334

7. Christen, M., Kern, A., Nikitchenko, A.,Steeb, W.-H., Stoop, R., 2004. Fast spike pattern detection using the correlation integral. PHYSICAL REVIEW E 70, 011901

8. Bennett, B.D., Wilson, C.J., 1999. Spontaneous Activity of Neostriatal Cholinergic Interneurons In Vitro. The Journal of Neuroscience, 19(13):5586–5596

9. Shi, W.-X., 2005. Slow Oscillatory Firing: A Major Firing Pattern of Dopamine Neurons in the Ventral Tegmental Area. J Neurophysiol 94: 3516 –3522

10. Lee, S. C., Deutsch, C., 1990. Temperature dependence of $K^+$-channel properties in human T lymphocytes. Biophys. J. e, Volume 57, 49-62

# 6 Appendix

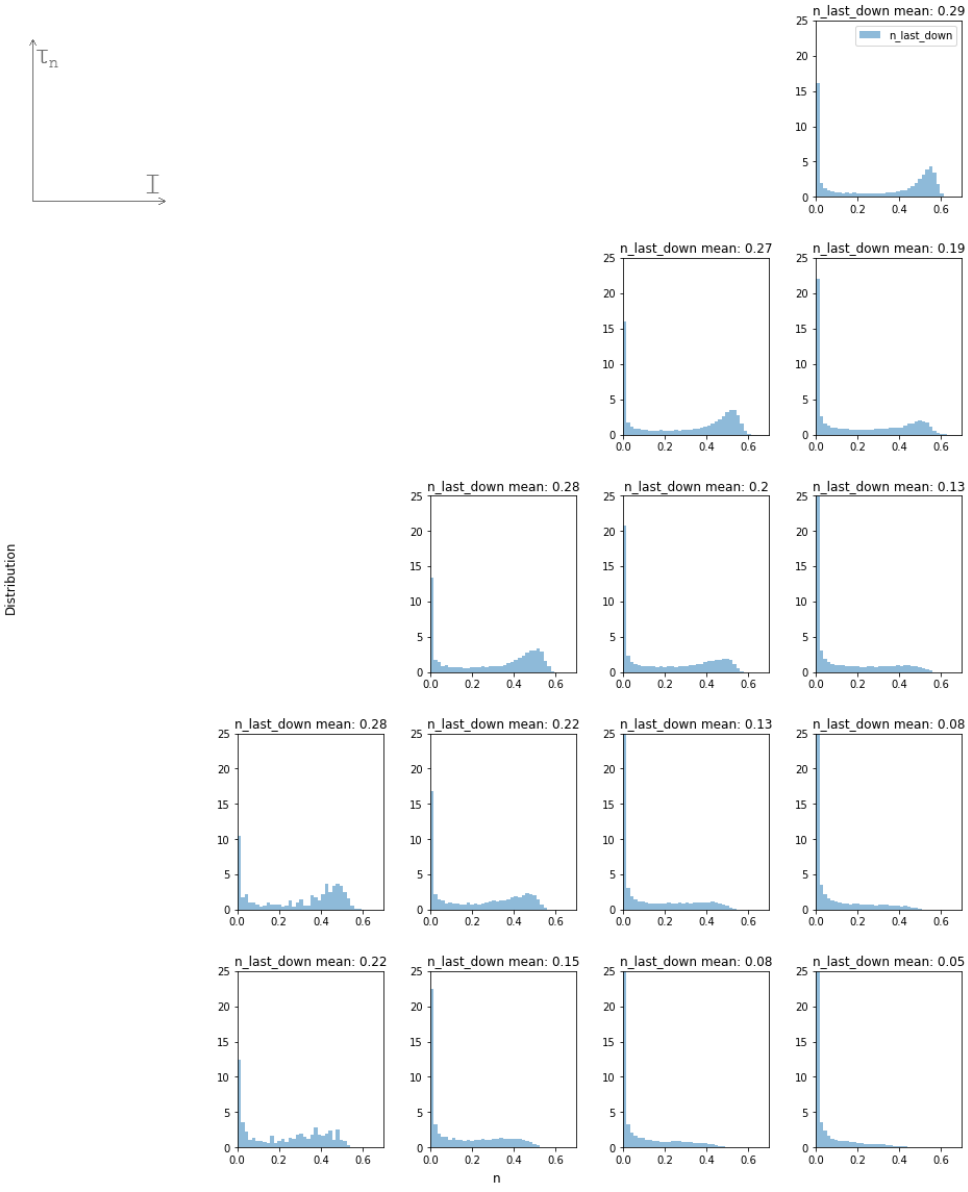


Figure 19: Distributions of $n$-values at "crossing down" points for the selected parameters' pairs and $\mu_{I_{noise}} = 2\mu\text{A}/cm^2$.

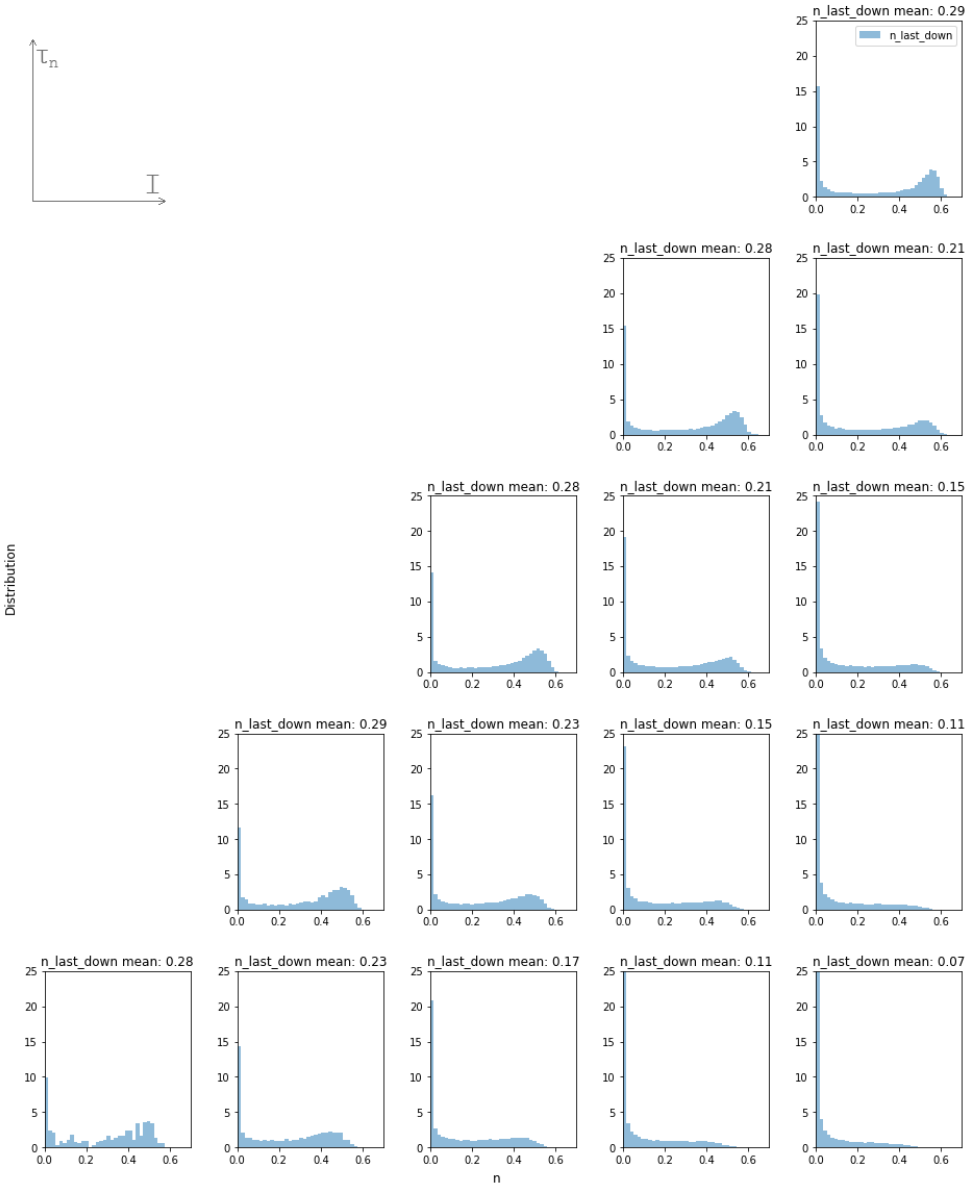


Figure 20: Distributions of $n$-values at "crossing down" points for the selected parameters' pairs and $\mu_{I_{noise}} = 2.5\mu\text{A}/cm^2$.

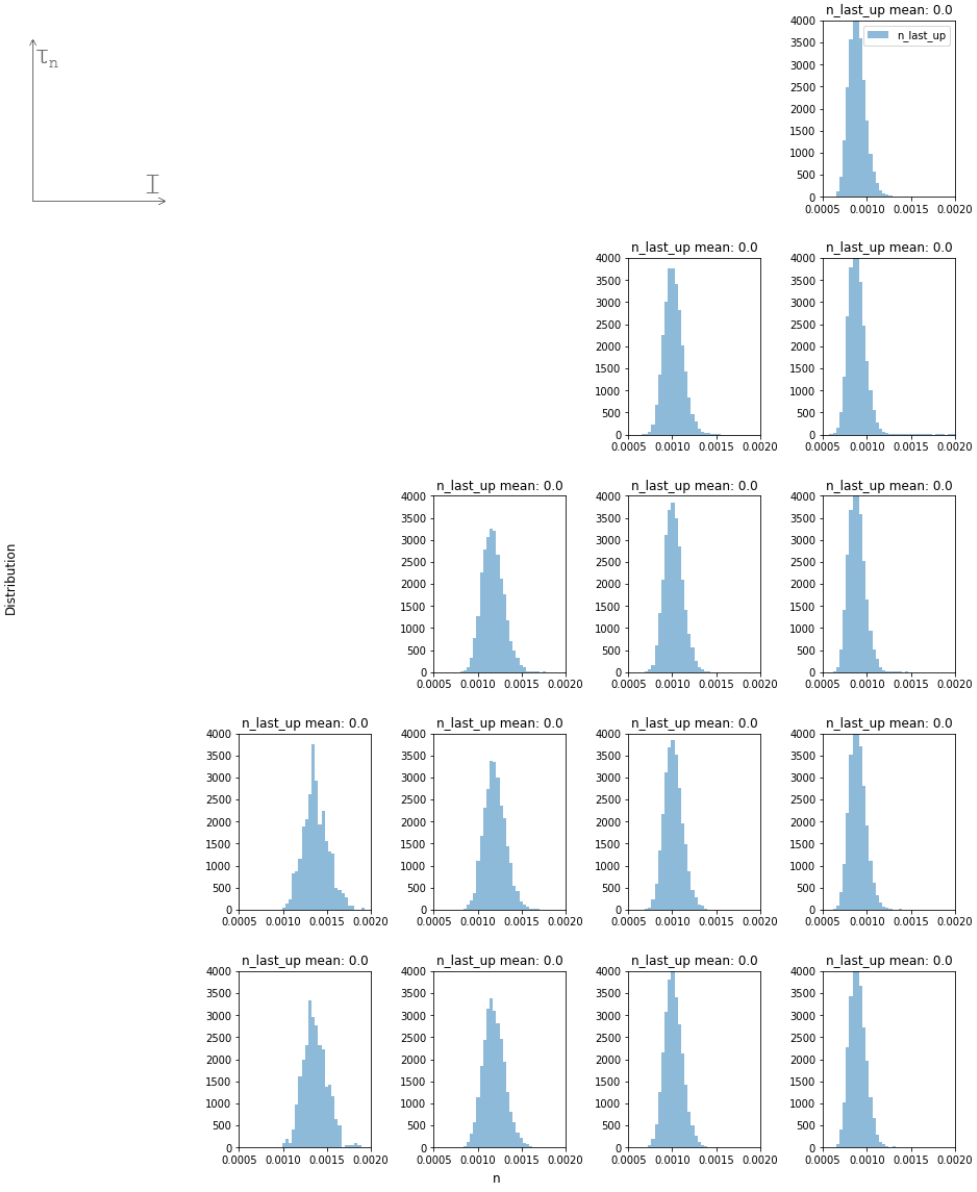


Figure 21: Distributions of $n$-values at "crossing up" points for the selected parameters' pairs and $\mu_{I_{noise}} = 2\mu\text{A}/cm^2$.

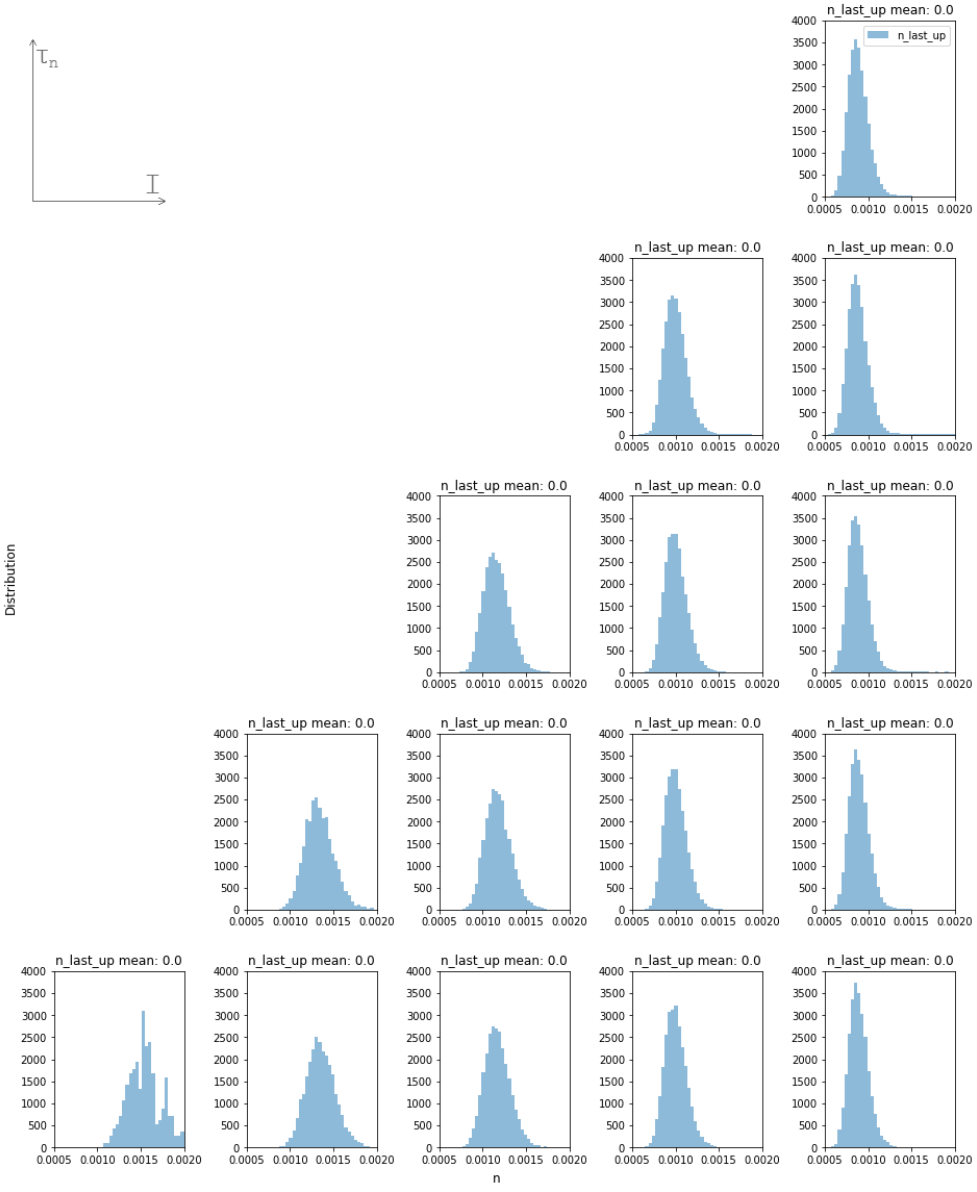


Figure 22: Distributions of $n$-values at "crossing up" points for the selected parameters' pairs and $\mu_{I_{noise}} = 2.5\mu\text{A}/cm^2$.

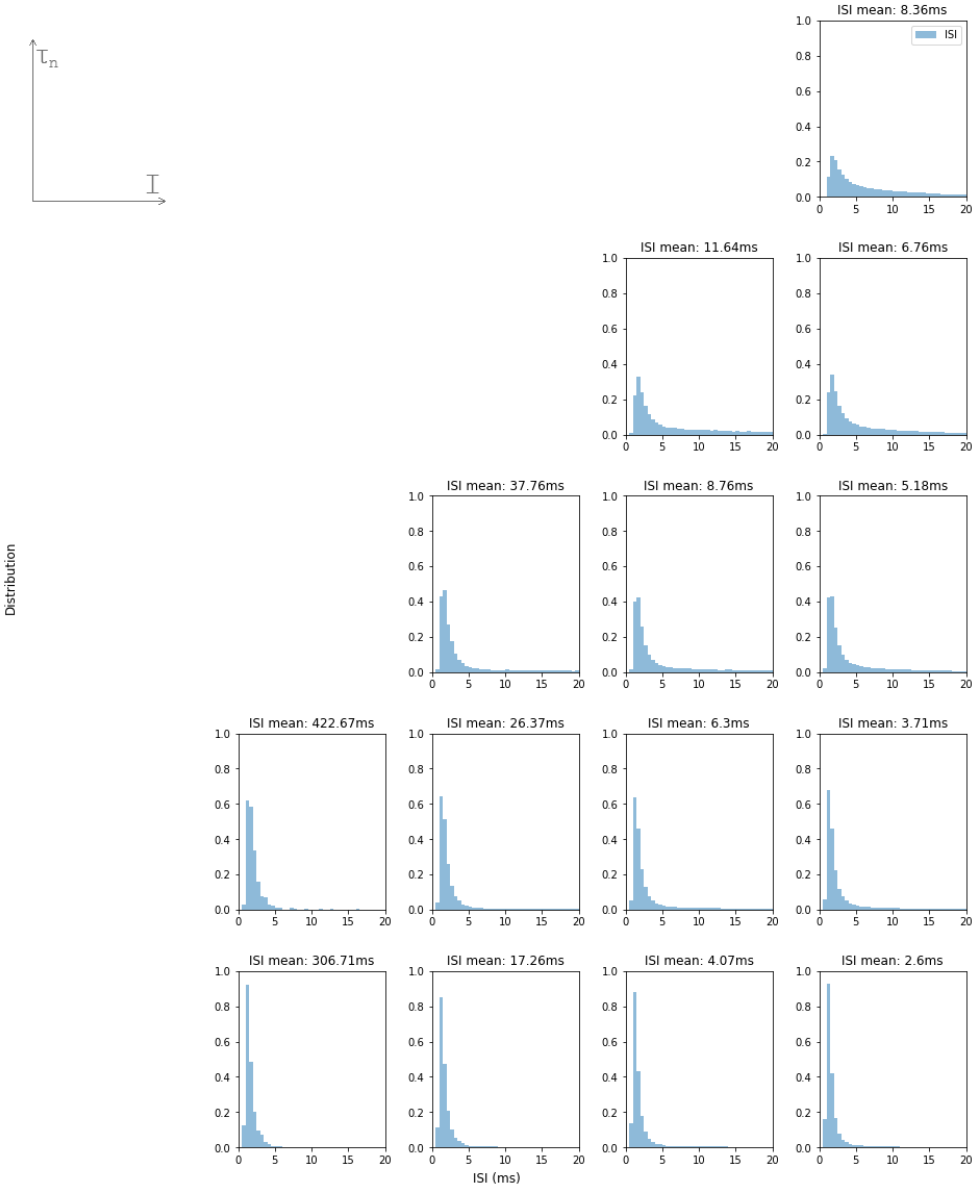


Figure 23: Overall distributions of ISIs for the selected parameters' pairs and $\mu_{I_{noise}} = 2\mu\text{A}/cm^2$.

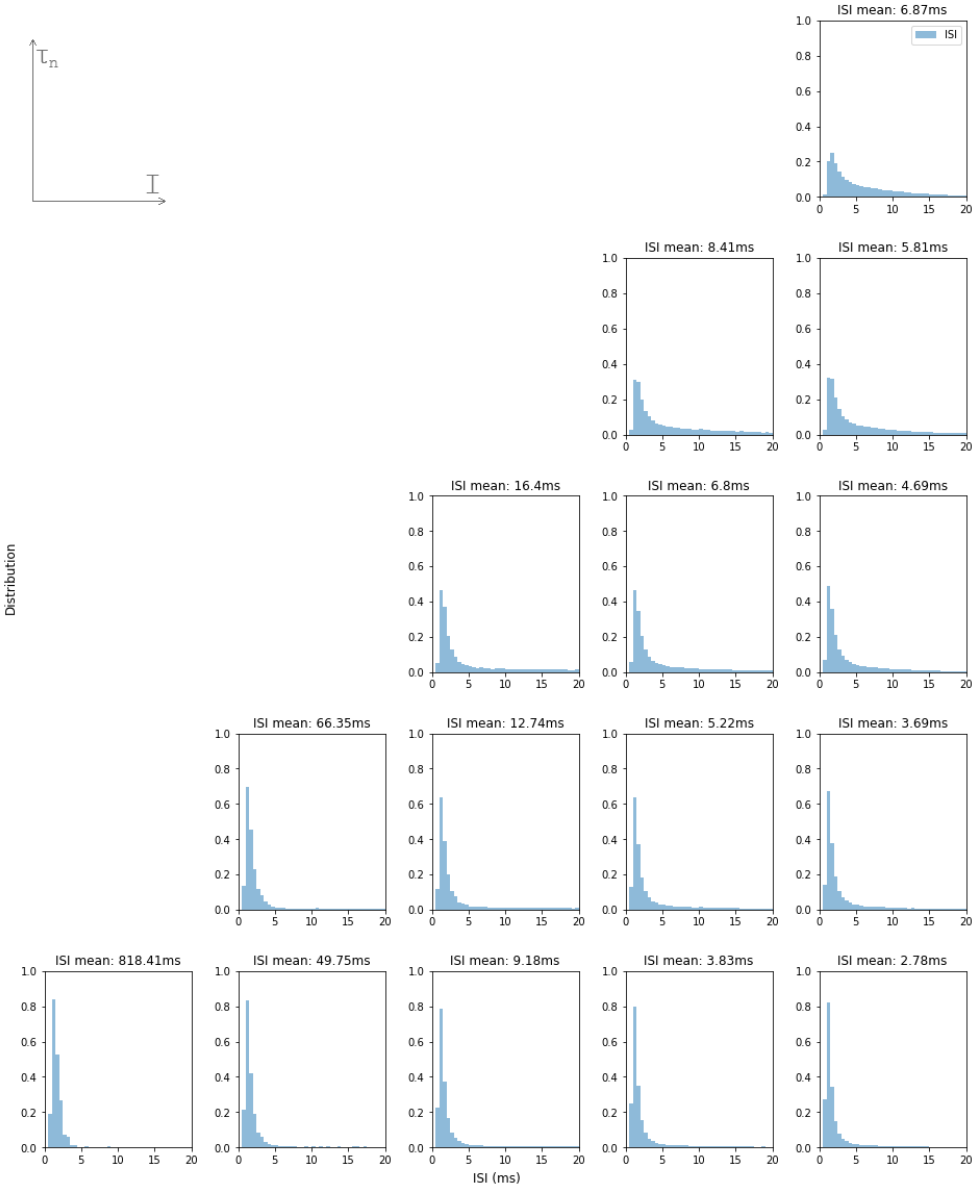


Figure 24: Overall distributions of ISIs for the selected parameters' pairs and $\mu_{I_{noise}} = 2.5\mu\text{A}/cm^2$.

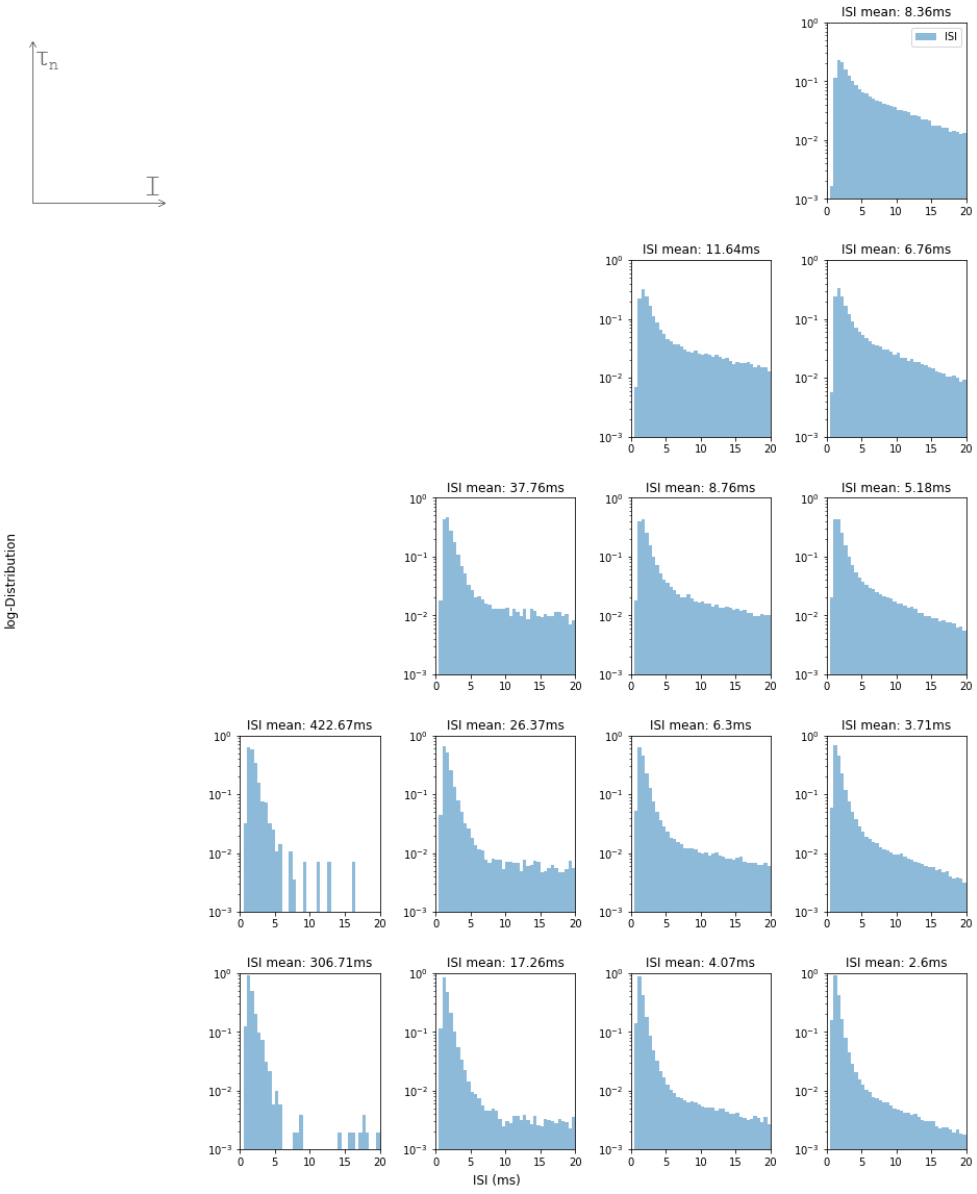


Figure 25: Overall log-distributions of ISIs for the selected parameters' pairs and $\mu_{I_{noise}} = 2\mu\text{A}/cm^2$.

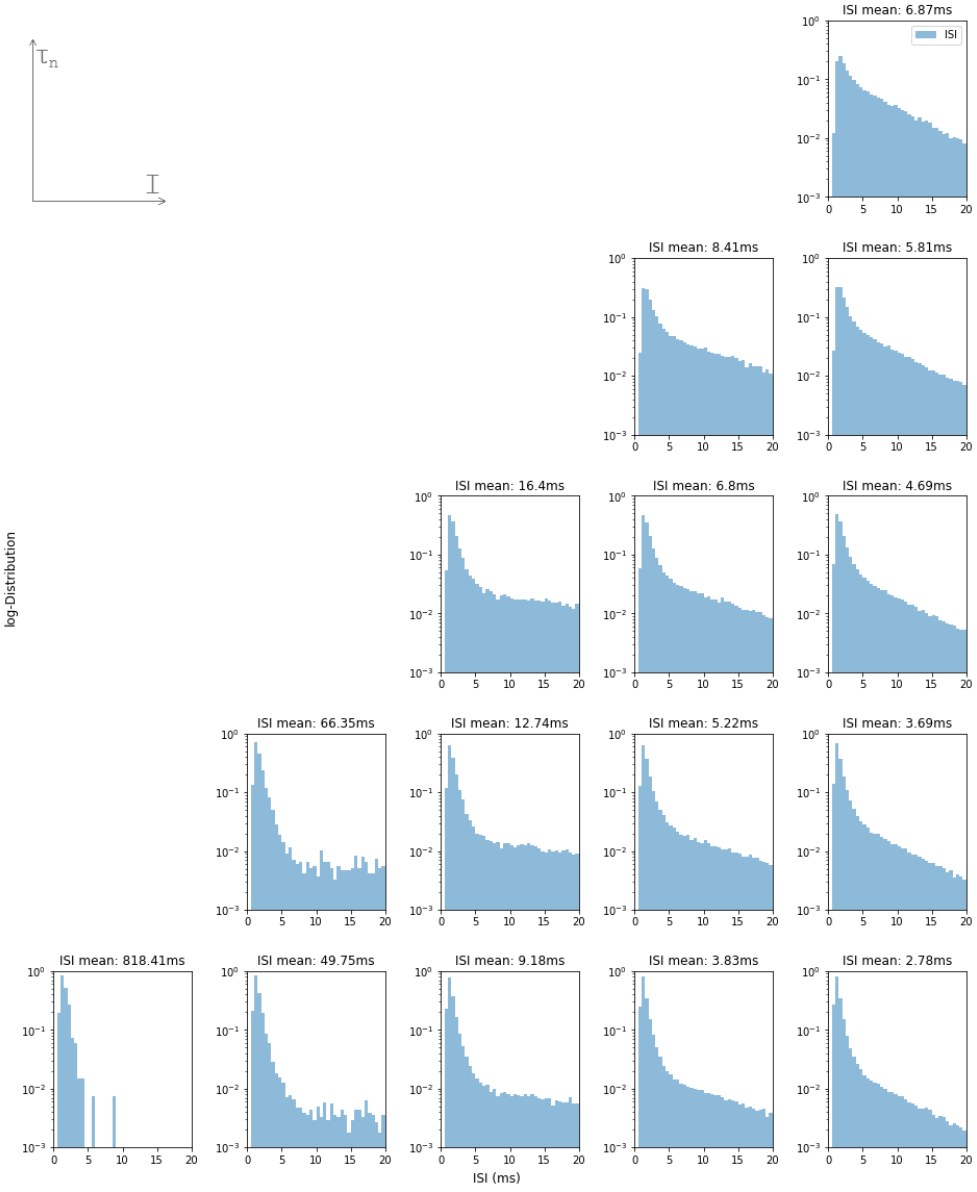


Figure 26: Overall log-distributions of ISIs for the selected parameters' pairs and $\mu_{I_{noise}} = 2.5\mu\text{A}/cm^2$.

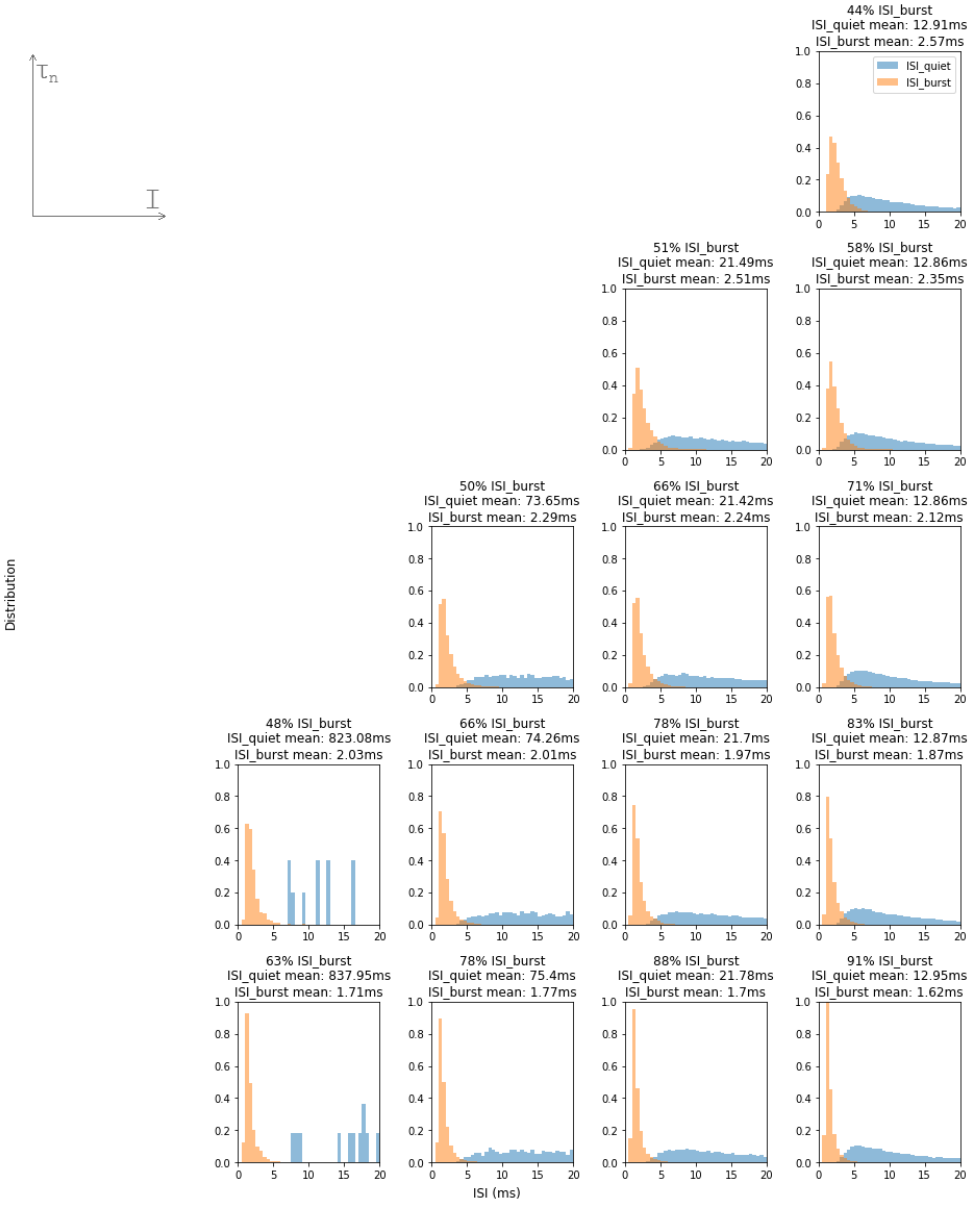


Figure 27: Distributions of quiet and burst ISIs for the selected parameters' pairs and $\mu_{I_{noise}} = 2\mu\text{A}/cm^2$.

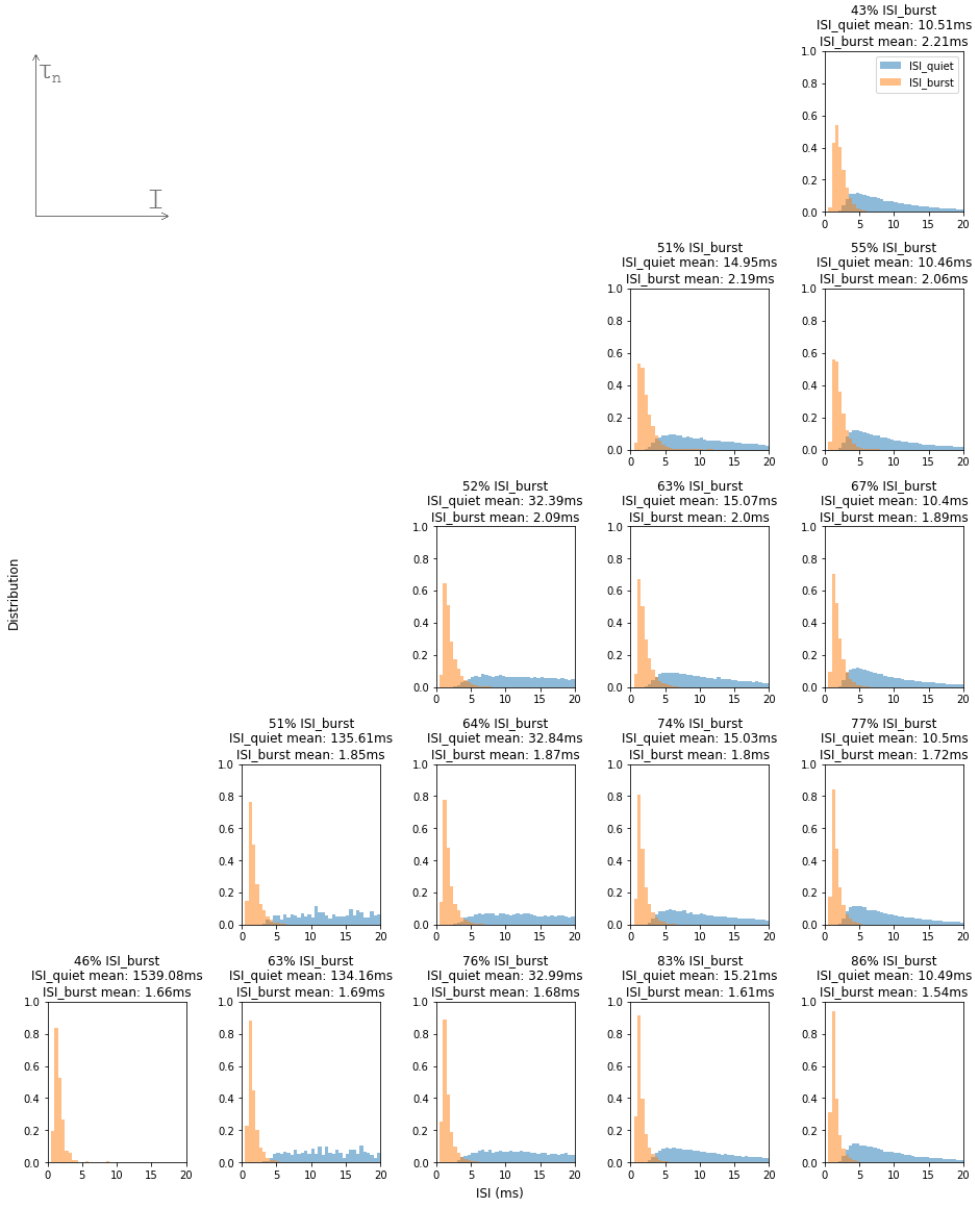


Figure 28: Distributions of quiet and burst ISIs for the selected parameters' pairs and $\mu_{I_{noise}} = 2.5\mu\text{A}/cm^2$.

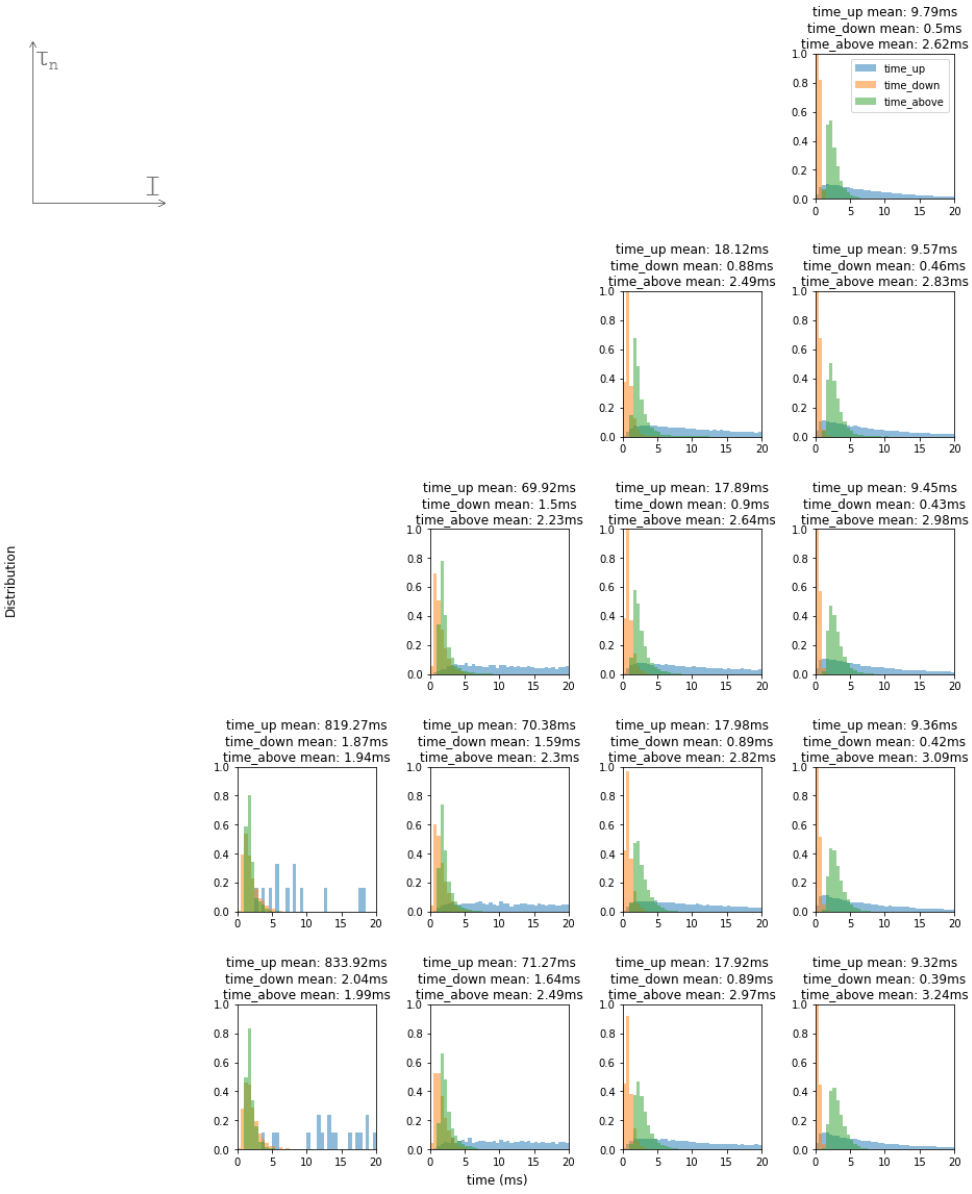


Figure 29: Distributions of quiet ISIs' segments for the selected parameters' pairs and $\mu_{I_{noise}} = 2\mu\text{A}/cm^2$.

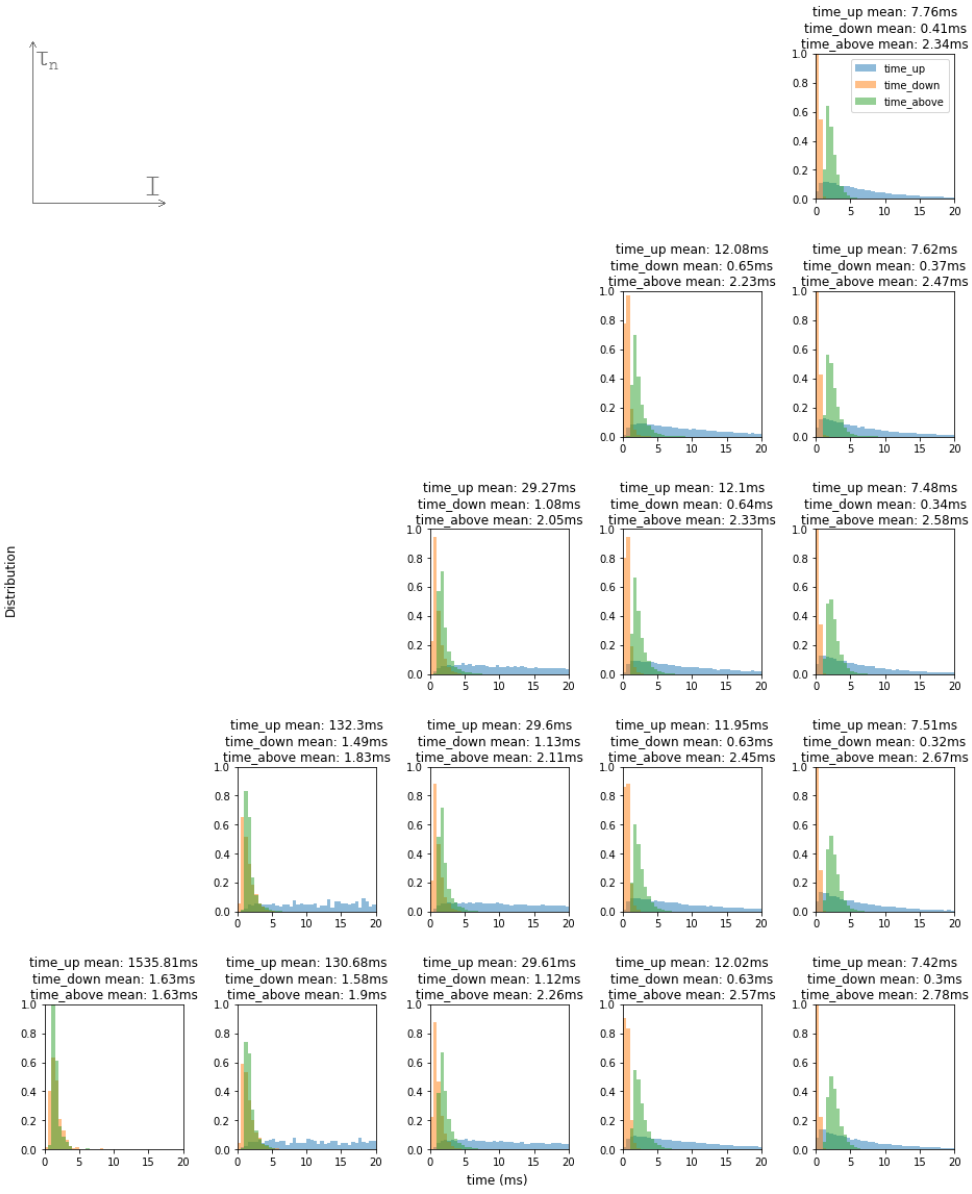


Figure 30: Distributions of quiet ISIs' segments for the selected parameters' pairs and $\mu_{I_{noise}} = 2.5\mu\text{A}/cm^2$.

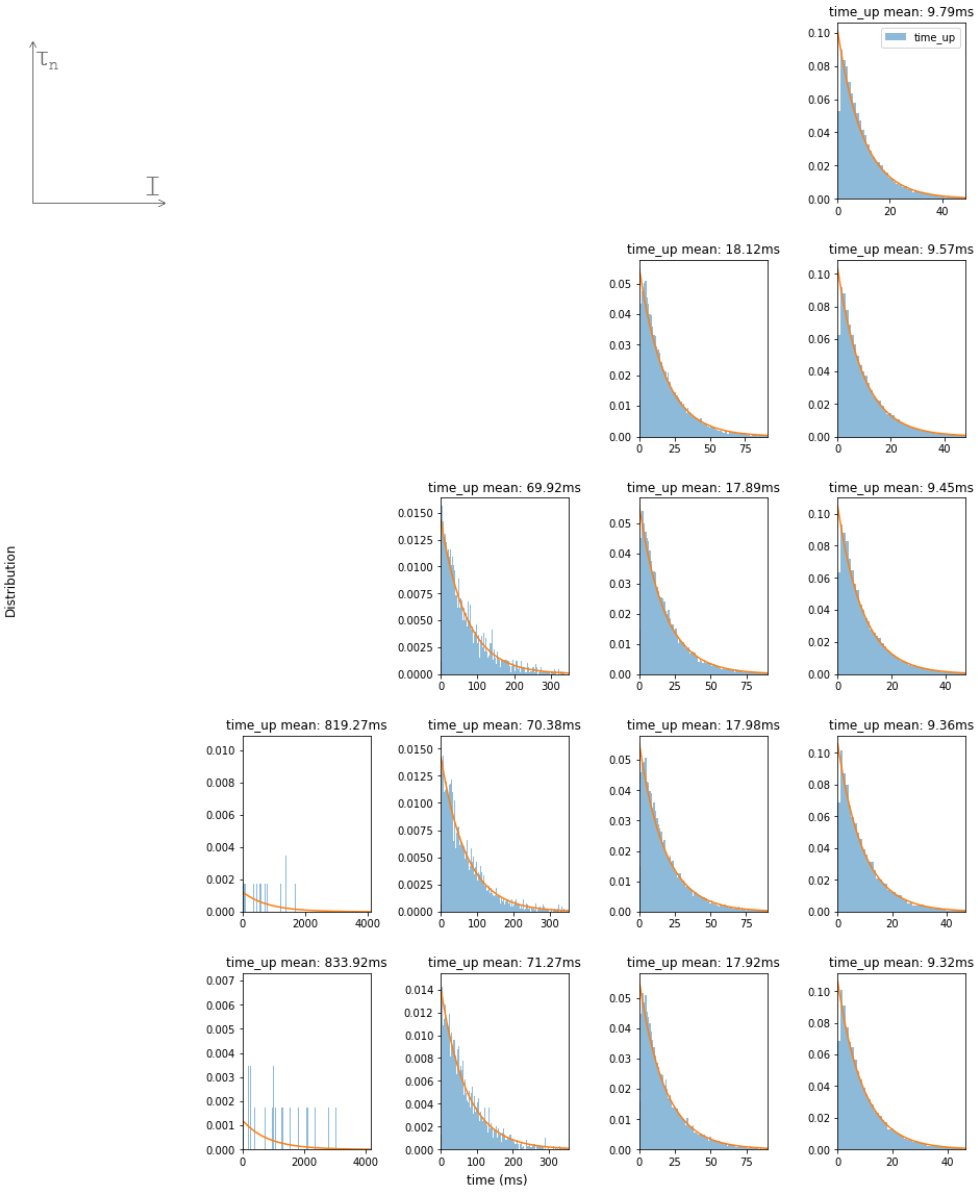


Figure 31: Distributions of "time up" and their exponential fits for the selected parameters' pairs and $\mu_{I_{noise}} = 2\mu\text{A}/cm^2$.

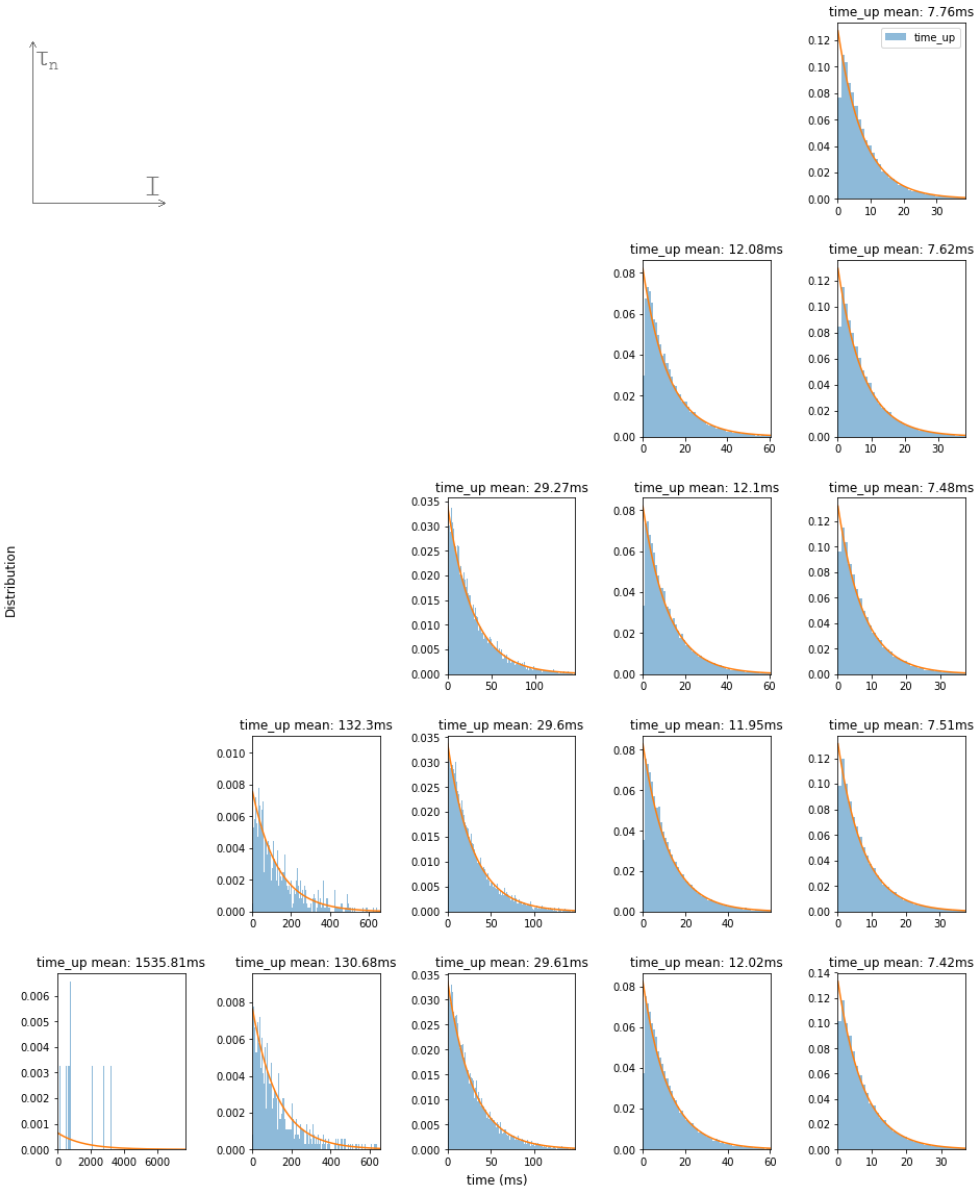


Figure 32: Distributions of "time up" and their exponential fits for the selected parameters' pairs and $\mu_{I_{noise}} = 2.5\mu\text{A}/cm^2$.

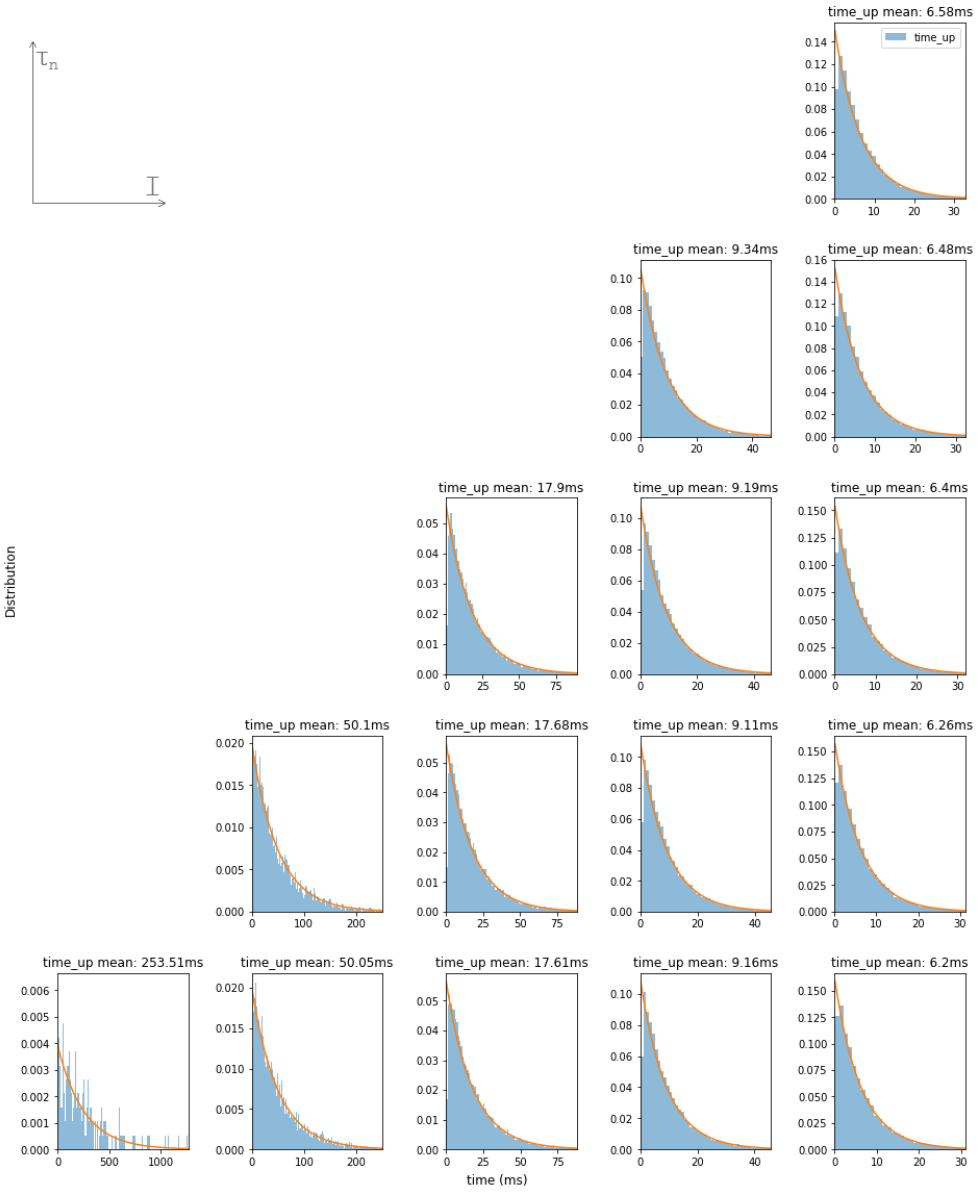


Figure 33: Distributions of "time up" and their exponential fits for the selected parameters' pairs and $\mu_{I_{noise}} = 3\mu\text{A}/cm^2$.

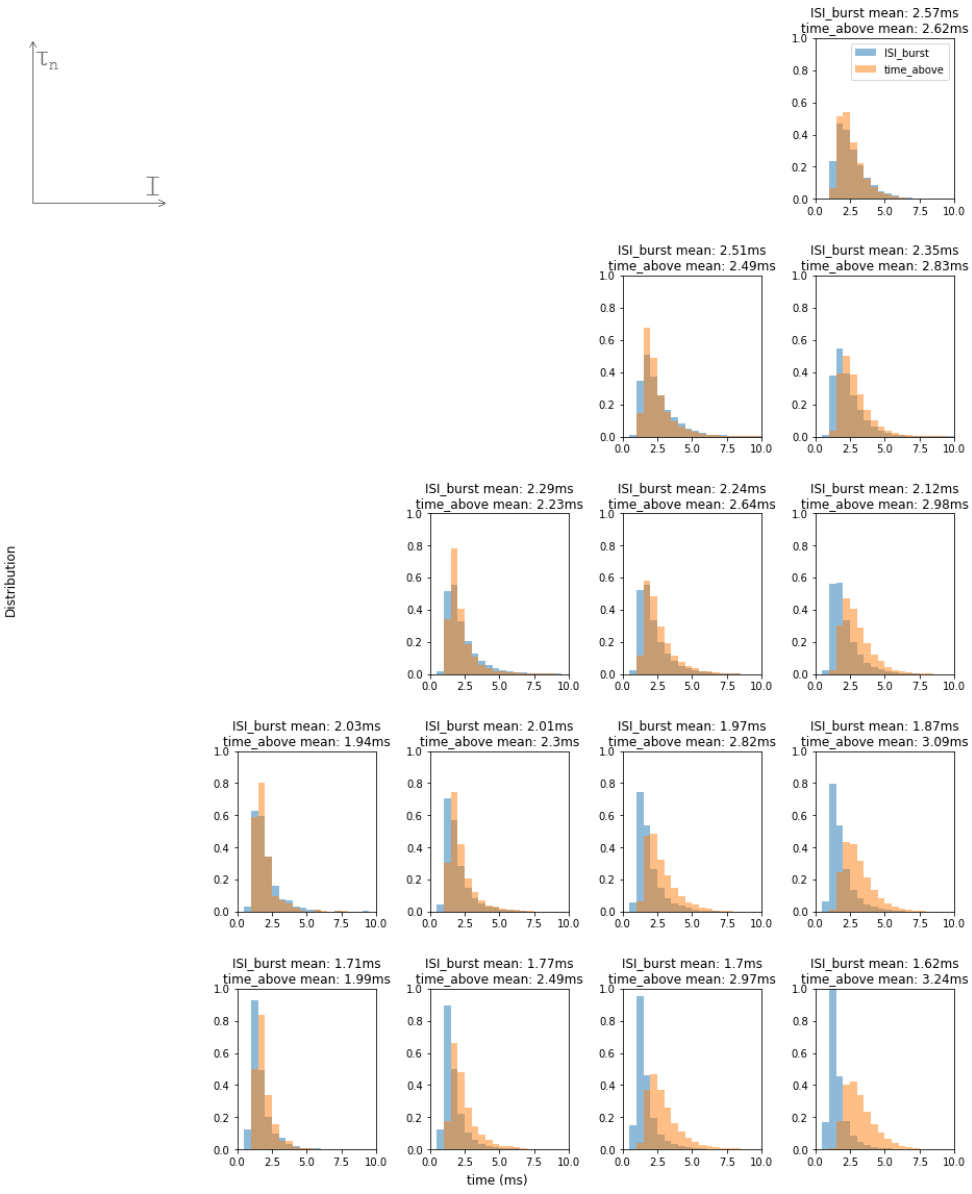


Figure 34: Distributions of burst ISIs and "time above" for the selected parameters' pairs and $\mu_{I_{noise}} = 2\mu\text{A}/cm^2$.

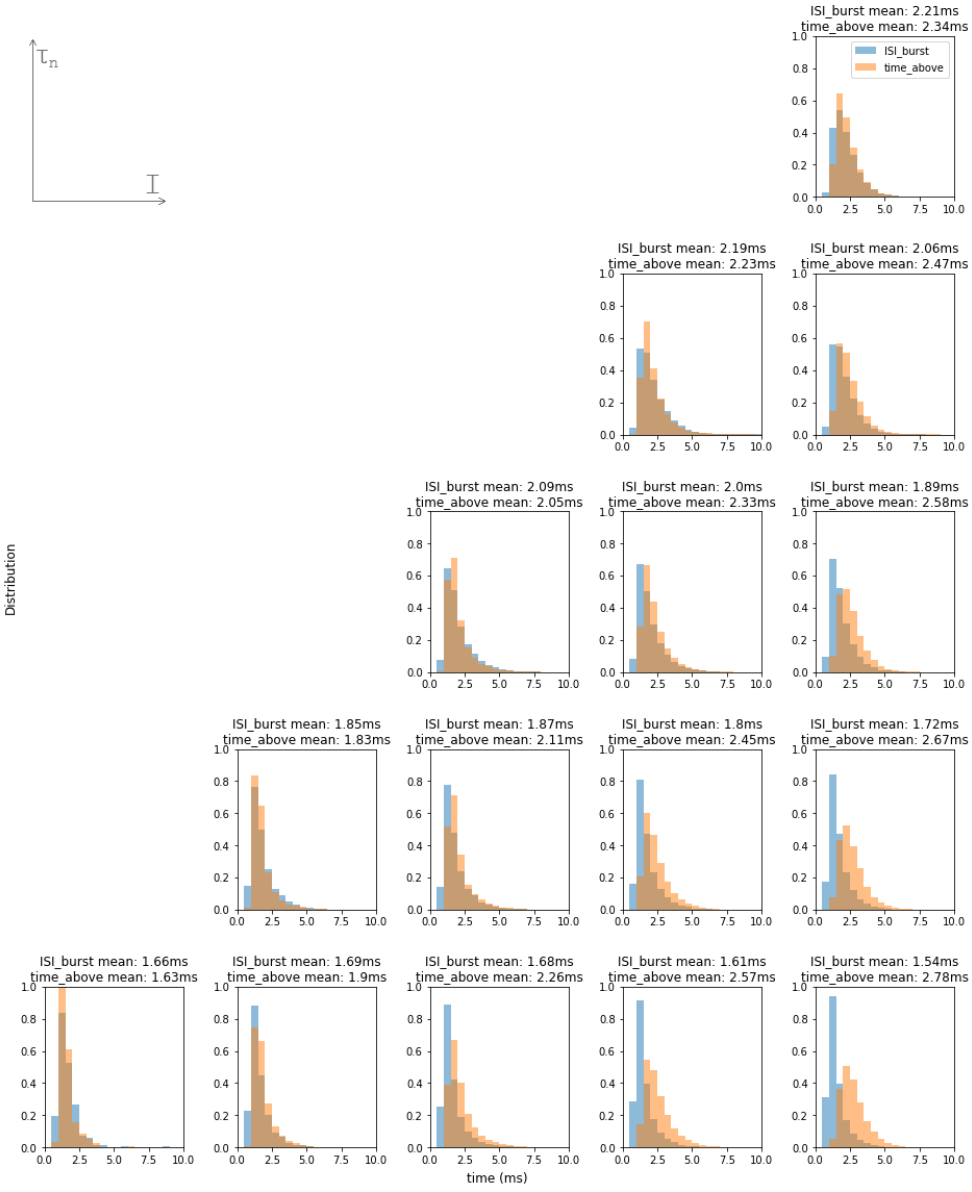


Figure 35: Distributions of burst ISIs and "time above" for the selected parameters' pairs and $\mu_{I_{noise}} = 2.5\mu\text{A}/cm^2$.

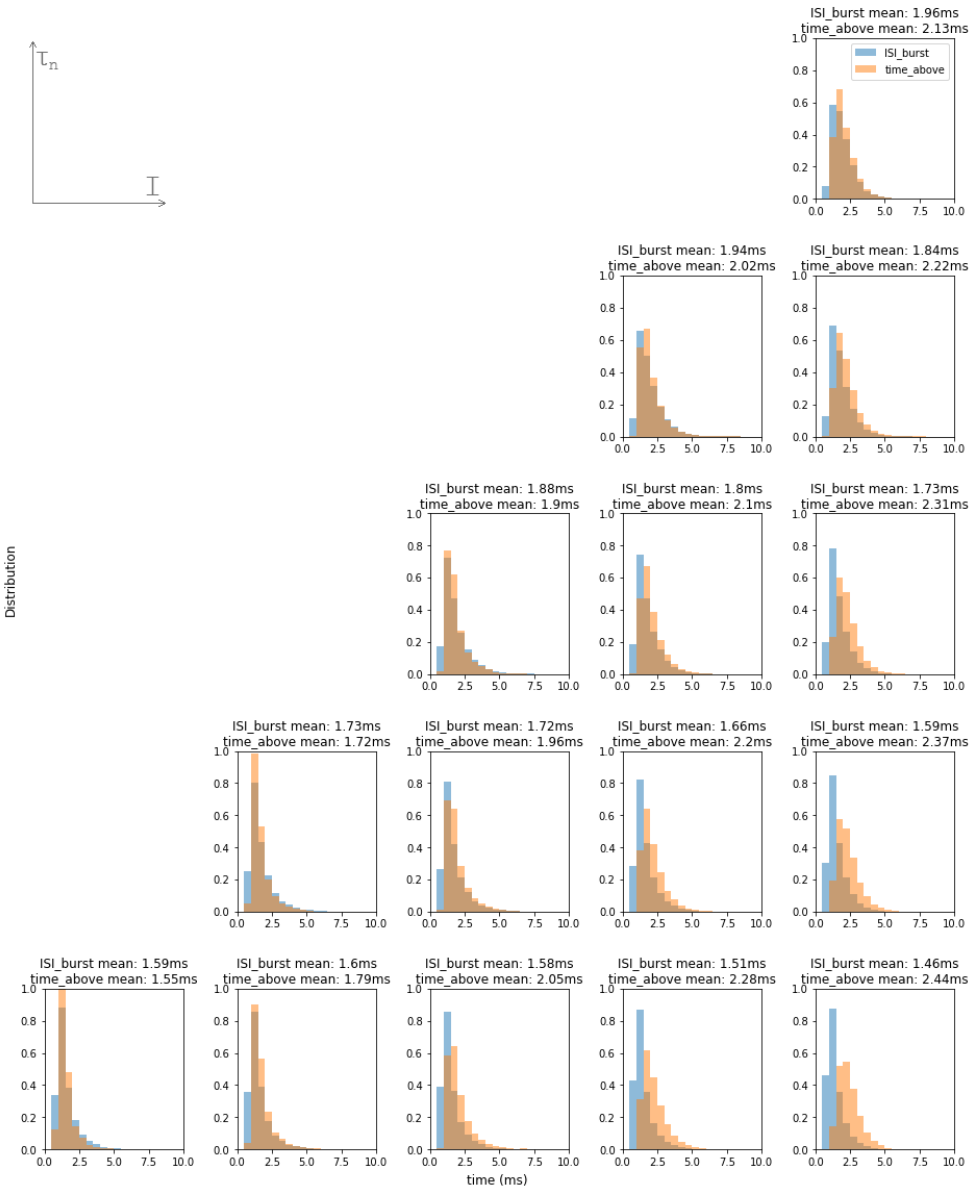


Figure 36: Distributions of burst ISIs and "time above" for the selected parameters' pairs and $\mu_{I_{noise}} = 3\mu\text{A}/cm^2$.

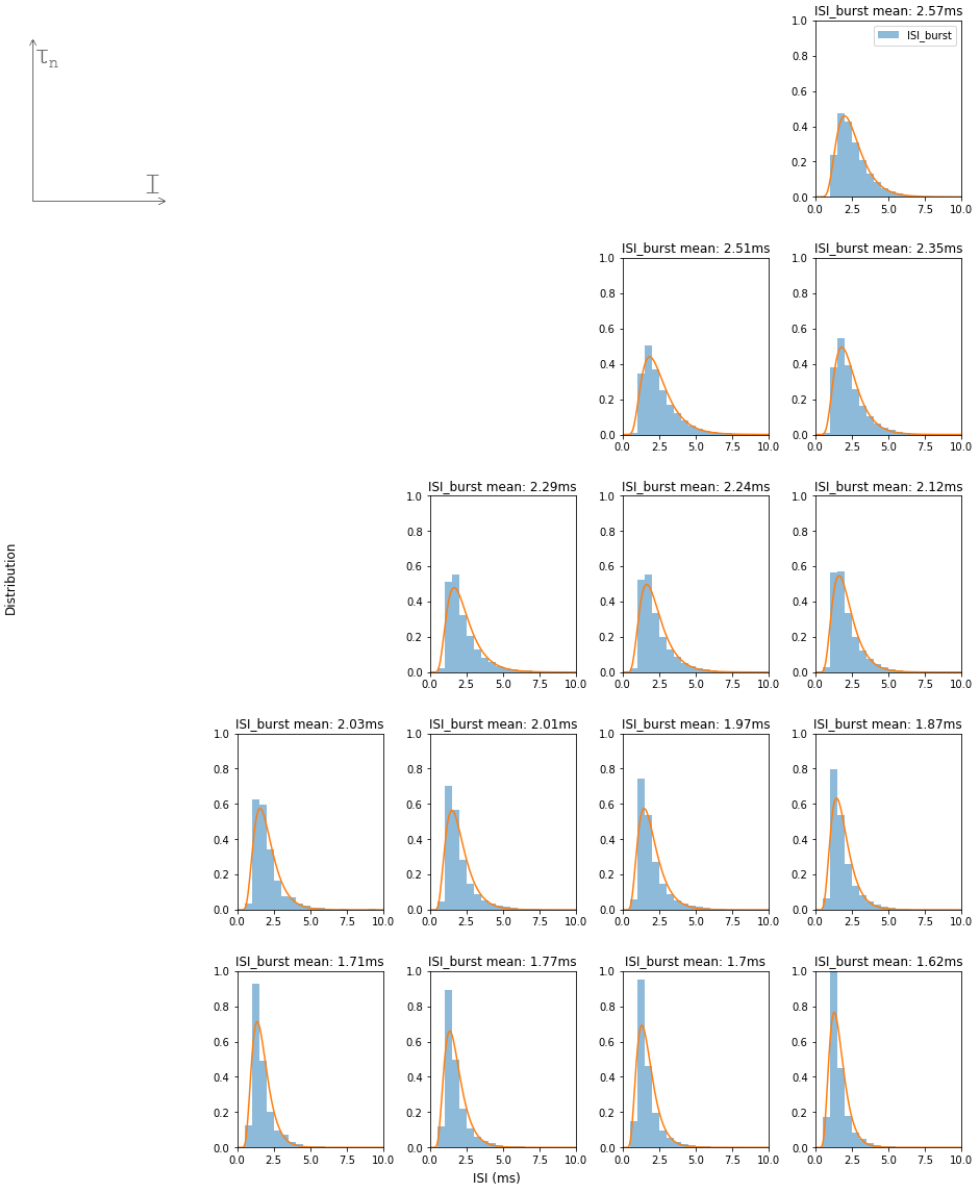


Figure 37: Distributions of burst ISIs and their inverse gaussian fits for the selected parameters' pairs and $\mu_{I_{noise}} = 2\mu\text{A}/cm^2$.

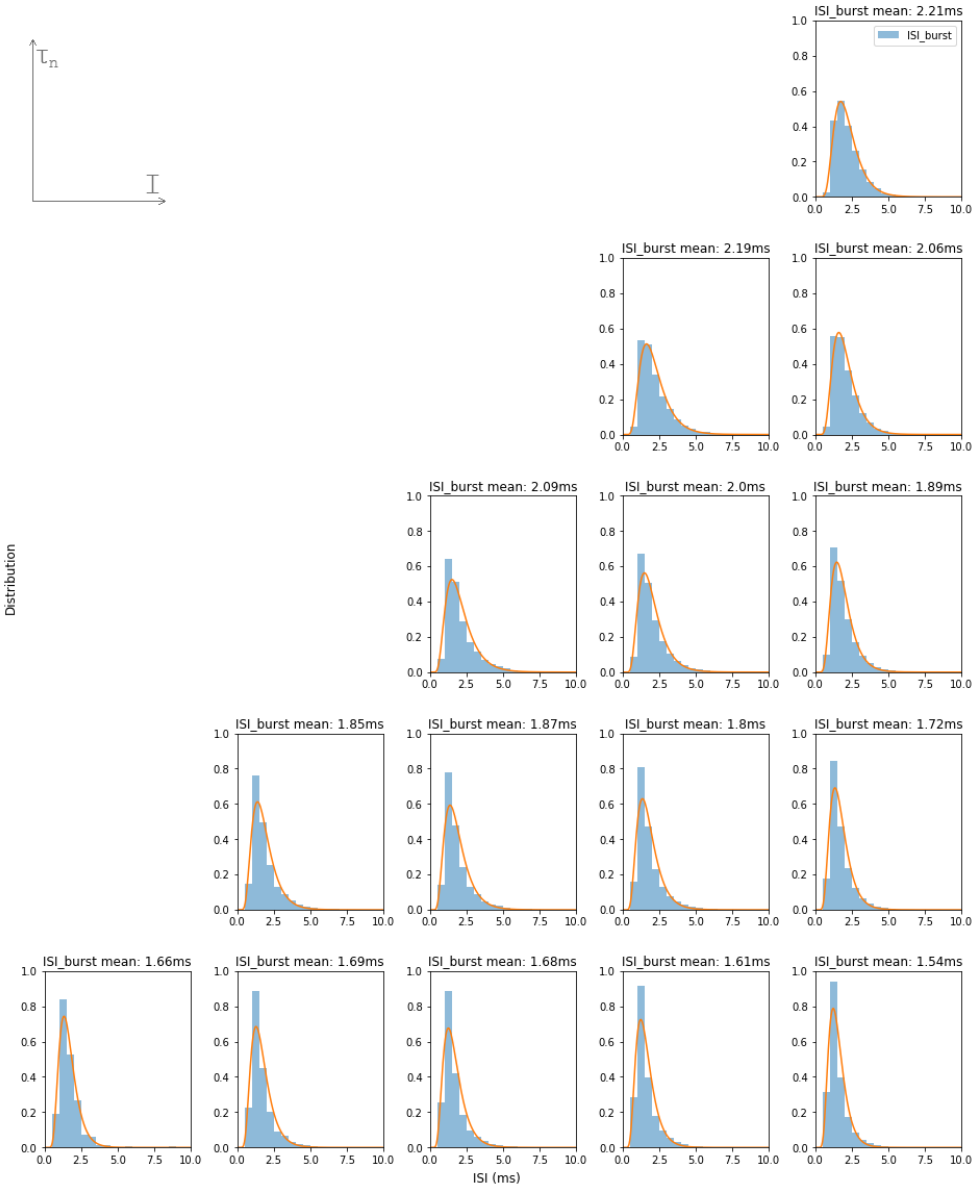


Figure 38: Distributions of burst ISIs and their inverse gaussian fits for the selected parameters' pairs and $\mu_{I_{noise}} = 2.5\mu\text{A}/cm^2$.

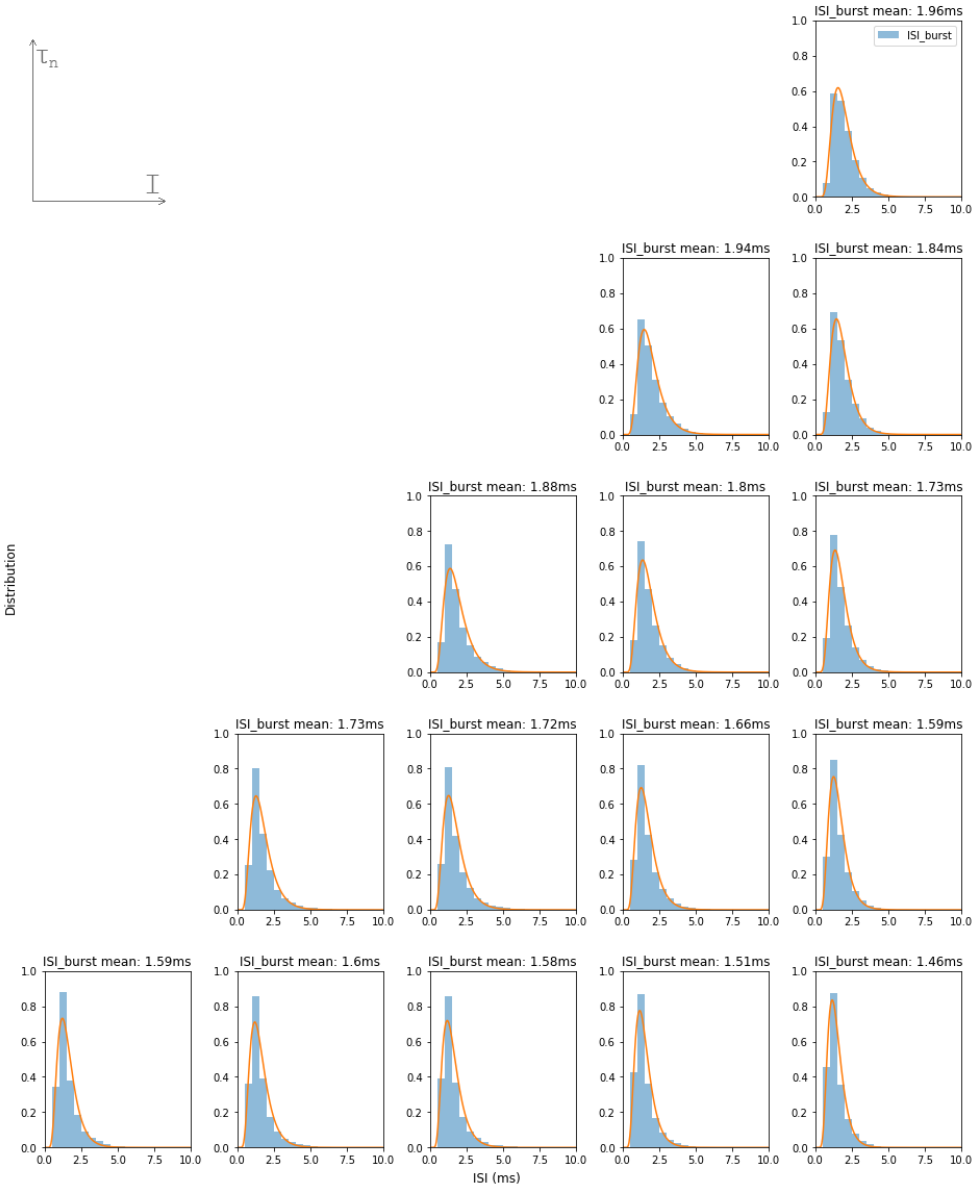


Figure 39: Distributions of burst ISIs and their inverse gaussian fits for the selected parameters' pairs and $\mu_{I_{noise}} = 3\mu\text{A}/cm^2$.

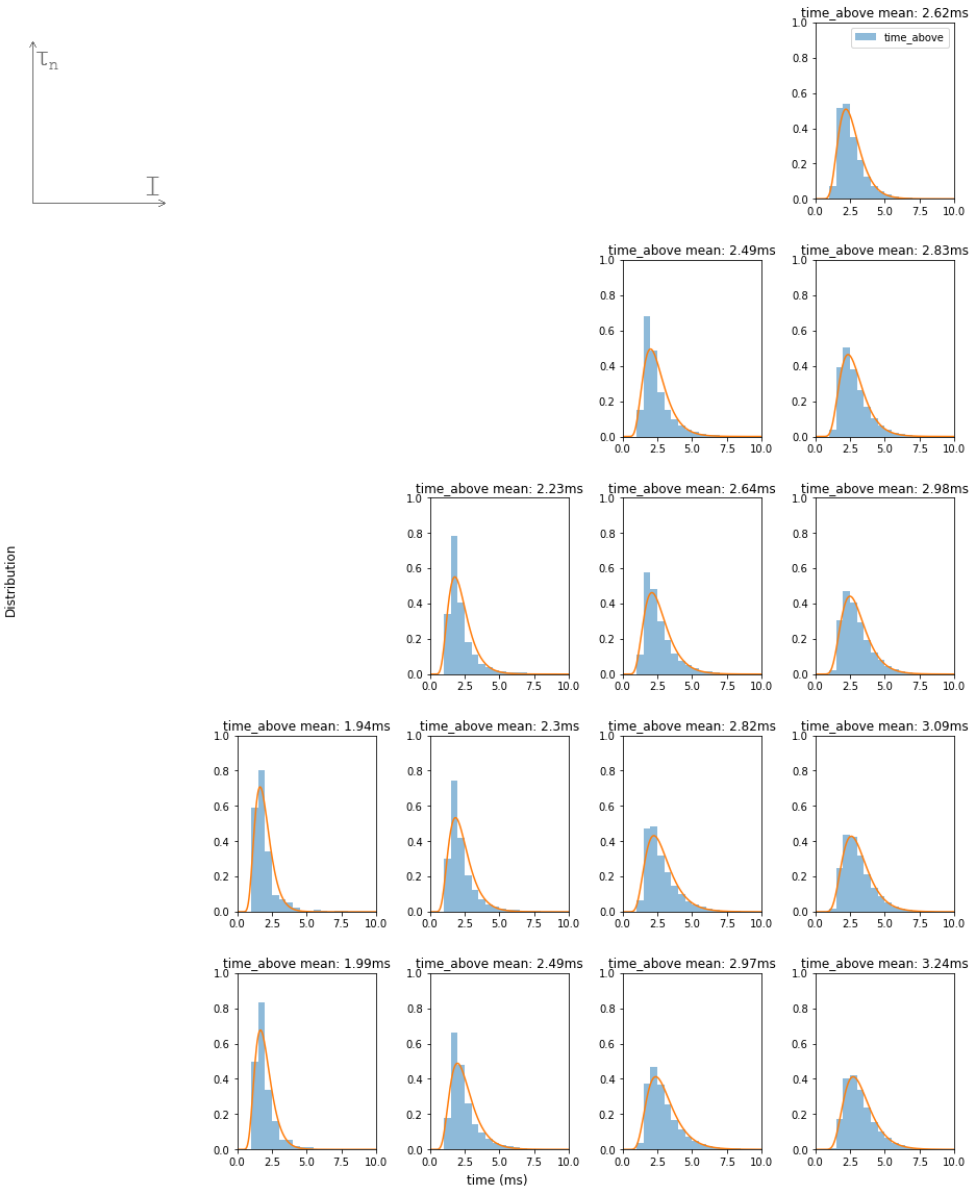


Figure 40: Distributions of "time above" and their inverse gaussian fits for the selected parameters' pairs and $\mu_{I_{noise}} = 2\mu\text{A}/cm^2$.

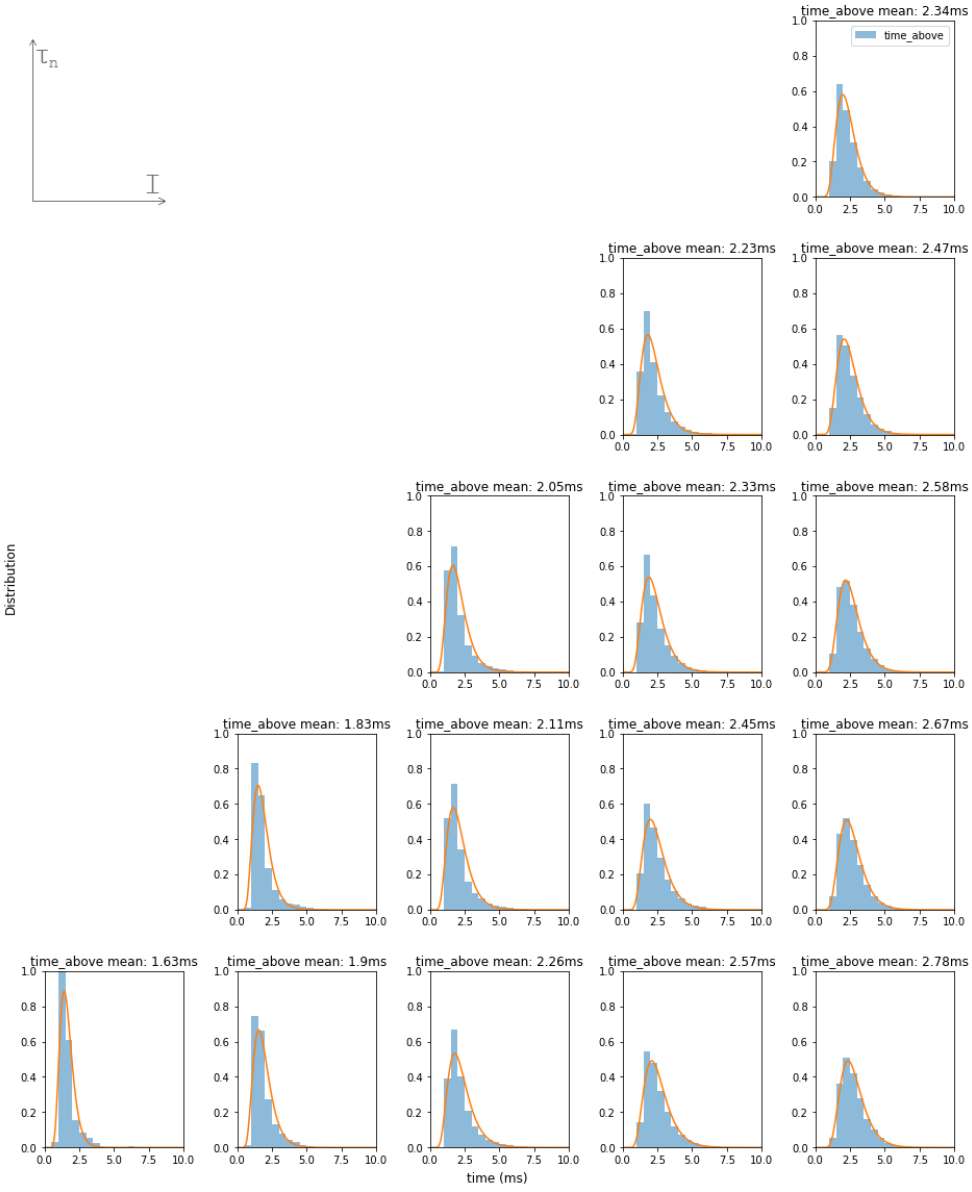


Figure 41: Distributions of "time above" and their inverse gaussian fits for the selected parameters' pairs and $\mu_{I_{noise}} = 2.5\mu\text{A}/cm^2$.

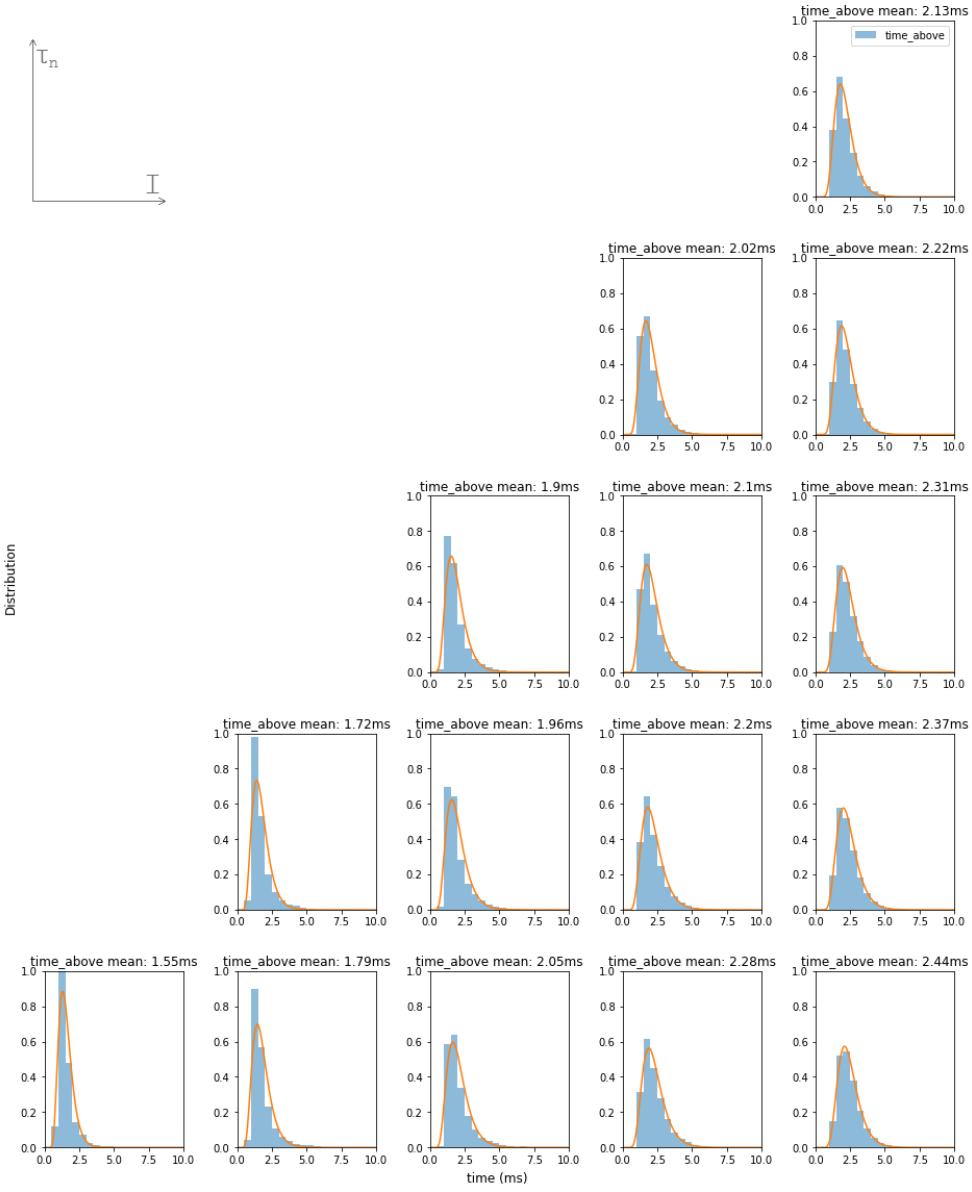


Figure 42: Distributions of "time above" and their inverse gaussian fits for the selected parameters' pairs and $\mu_{I_{noise}} = 3\mu\text{A}/cm^2$.